Received: 31 October 2022 | Revised: 22 February 2023 | Accepted: 19 March 2023

DOI: 10.1002/nme.7244

RESEARCH ARTICLE

WILEY

On the effectiveness of the Moulinec–Suquet discretization for composite materials

Matti Schneider

Institute of Engineering Mechanics, Karlsruhe Institute of Technology (KIT), Karlsruhe, Germany

Correspondence
Matti Schneider, Institute of Engineering Mechanics, Karlsruhe Institute of Technology (KIT), Karlsruhe, Germany.
Email: matti.schneider@kit.edu

Funding information
Deutsche Forschungsgemeinschaft, Grant/Award Number: 255730231; European Research Council within the Horizon Europe, Grant/Award Number: 101040238; European Research Council

Abstract

Moulinec and Suquet introduced a method for computational homogenization based on the fast Fourier transform which turned out to be rather computationally efficient. The underlying discretization scheme was subsequently identified as an approach based on trigonometric polynomials, coupled to the trapezoidal rule to substitute full integration. For problems with smooth solutions, the power of spectral methods is well-known. However, for heterogeneous microstructures, there are jumps in the coefficients, and the solution fields are not smooth enough due to discontinuities across material interfaces. Previous convergence results only provided convergence of the discretization per se, that is, without explicit rates, and could not explain the effectiveness of the discretization observed in practice. In this work, we provide such explicit convergence rates for the local strain as well as the stress field and the effective stresses based on more refined techniques. More precisely, we consider a class of industrially relevant, discontinuous elastic moduli separated by sufficiently smooth interfaces and show rates which are known to be sharp from numerical experiments. The applied techniques are of independent interest, that is, we employ a local smoothing strategy, utilize Féjer means as well as Bernstein estimates and rely upon recently established superconvergence results for the effective elastic energy in the Galerkin setting. The presented results shed theoretical light on the effectiveness of the Moulinec–Suquet discretization in practice. Indeed, the obtained convergence rates coincide with those obtained for voxel finite element methods, which typically require higher computational effort.

KEYWORDS

computational homogenization, convergence estimate, FFT-based methods, non-smooth coefficients, spectral method

1 | INTRODUCTION

1.1 | State of the art

Computational homogenization methods[1] may be used to reduce the experimental effort required to characterize heterogeneous materials. To ensure compatibility with modern image-processing tools,[2,3] numerical methods on regular grids were established as the de-facto standard tool in computational micromechanics. Moulinec and Suquet[4,5] introduced

a computational method to solve the cell problem of homogenization which is based on the fast Fourier transform (FFT) as an efficient alternative to more classical numerical approaches, for example, based on a finite element discretization.

In its original form, FFT-based computational micromechanics involved essentially three ingredients—a class of models to be treated, a discretization and a solver. The original Moulinec–Suquet method was designed to handle quasistatic mechanical problems at small strains. In particular, inelastic problems were in the focus right from the beginning. In a continuous effort, researchers extended the domain of applicability, for example, towards problems at finite strains[6-8] or coupled problems.[9-11] We refer to the review articles[12-14] for a glimpse at the numerous applications of this class of numerical methods.

These developments were complemented by extensions of the original solution scheme of Moulinec–Suquet which they termed the *basic scheme*. The latter was based on the weak-contrast expansion well-known in micromechanics[15,16] which itself derives from series representations[17,18] of effective properties in the material contrast established with the help of the Lippmann–Schwinger equation.[19-21] A key advantage of the basic scheme is its low memory demand—there are implementations which require only a single strain field in memory.[22,23] Over the years, faster solution methods were introduced, usually at the cost of a higher memory footprint. Eyre and Milton[24] introduced a numerical method similar to the basic scheme but with higher convergence rate. To be more precise, the method has a link to the strong-contrast expansion[25,26] and may be written as a series expansion in the *square root* of the contrast, which is responsible for the faster convergence behavior. The original method was restricted to linear problems. Subsequently, modifications of the Eyre–Milton method were introduced[27-29] which applied to inelastic materials in a hardening regime[30,31] or problems of fracture mechanics.[32-34]

The caveat of these so-called polarization methods is the need to evaluate the constitutive law in a nonstandard way, and only for specific cases tricks are known to reduce the inherent effort considerably.[35,36] For this reason, also more traditional computational techniques were made available in the context of FFT-based methods, like Newton's method,[6,7,37] the (linear and nonlinear) conjugate gradient method[38,39] and a list of Quasi-Newton methods.[40-42] In particular, users of FFT-based methods may select a solver appropriate to their task at hand depending on the available resources and their performance demands, see the review article[14] for background and recommendations.

The extensions of applicability and solver technology were complemented by developments in discretization methods. To be more precise, there were essentially two lines of thought which were followed. On the one hand, the original Moulinec–Suquet method led to stress and strain fields which showed characteristic ringing artifacts in the vicinity of material interfaces. This so-called Gibbs phenomenon[43] is well-known in Fourier methods and reflects the limited ability of classical Fourier series to represent discontinuous functions. To remove these oscillations, different discretization methods were exploited, for example, finite difference,[44-46] finite element,[47-49] and finite volume[50,51] methods. The underlying key observation is that translation-invariant stencils of finite difference operators may be block-diagonalized in Fourier space, thus giving rise to a simple preconditioning strategy reminiscent of the original Moulinec–Suquet method. In particular, the developed solver technology could be transferred to this extended setting essentially without change. As an added benefit, it was observed that problems involving pores[52-54] or rigid inclusions[55,56] could be handled by dedicated discretization schemes which was difficult for the original Fourier-type discretization due to an intrinsic numerical instability related to the global support of the ansatz functions.[57]

The second line of thought on discretization methods involved understanding the discretization underlying the original Moulinec–Suquet method. This was motivated, on the one hand, by the idea that understanding is key to improvement, and, on the other hand, by the desire to create methods which provide upper and lower bounds on the effective properties. To obtain bounds, the classical strategy to minimize the average strain energy over compatible strain fields leads to the Fourier-Galerkin method[58-61] when using trigonometric polynomials as the ansatz space. A similar strategy may be applied to minimize the complementary energy over self-equilibrated stress fields,[62] leading to computable lower bounds[59,61] of the effective elastic energy. Alternatively, the variational principle of Hashin and Shtrikman[63-65] may be used to compute upper and lower bounds to the effective elastic properties. Brisard and Dormieux[22,66] pioneered such an approach based on voxel-wise constant strains, later extended to B-spline ansatz functions.[67] Both variational principles were used as the point of departure for *interpreting* the original Moulinec–Suquet discretization. Brisard and Dormieux regarded the original scheme as a nonconforming version of their Galerkin method of Hashin–Shtrikman type and gave the first convergence proof[66] for the former. Their proof relied upon voxel-wise homogeneous stiffnesses that were obtained by a specific averaging method that inspired the composite voxel technology.[68-70] Vondřejc et al.[71] introduced another interpretation of the Moulinec–Suquet discretization as an underintegrated Fourier-Galerkin method where the underintegration arises from applying the trapezoidal rule. They also provided a convergence proof which—in contrast

to Brisard and Dormieux[66]—required the coefficients of elasticity to be sufficiently smooth. These rather restrictive assumptions were subsequently removed. More precisely, convergence was established for merely Riemann integrable, that is, measurable and bounded, coefficients of elasticity. Moreover, a class of nonlinear elastic constitutive laws[72] was possible to be treated, all without the need for any averaging close to the interface.

Several years after these results, Ye and Chung[73] provided a fresh perspective on the convergence analysis of FFT-based computational micromechanics. They established convergence of the Moulinec–Suquet discretization, the discretization on a rotated staggered grid[46] and for trilinear finite elements.[47,48] Their analysis of the Moulinec–Suquet discretization involved an appropriate smoothing operator, allowing them to incorporate essentially arbitrary composite-voxel methods.[68-70] In the same paper, they provided a convergence proof for the discretization on a rotated staggered grid pioneered by Willot[46] based on an ingenious coordinate transformation in Fourier space which emphasizes the connections to the non-conforming $P1$-quadrilateral elements introduced by Park and Sheen.[74] In addition to the mentioned qualitative convergence statements, Ye and Chung[73] also provided quantitative estimates for the convergence rate of a finite element discretization on a regular grid. More precisely, they showed that the strain field converges as $N^{-1/2}$ in L^2 where N denotes the number of voxels per edge. A similar convergence rate is known when approximating *outer boundaries* with Cartesian finite elements,[75] so that the rate $N^{-1/2}$ did not come as a surprise for methods which approximate *inner boundaries* on regular grids. However, Ye and Chung[73] also provided the insight that the *effective stresses* converge as $1/N$, that is, with the quadratic rate of the local fields.

Based on Ye–Chung's observation, it was shown that this phenomenon of higher order convergence of effective stresses also holds for inelastic problems and Galerkin discretizations.[76] Moreover, it was shown that a clever averaging procedure may increase the accuracy of the computed effective stresses significantly[77] by using the insights of Ye and Chung[73] appropriately.

1.2 | Contributions

The starting point of this article was the Ye–Chung superconvergence result[73] for the effective stress and its inelastic generalization.[76] In its simplest form, the higher-order rate for the effective stresses follows directly from Galerkin orthogonality. It was empirically observed by many authors that non-conforming discretizations, in particular based on underintegration, typically outperform Galerkin discretizations. However, their analysis is more involved, as the effect of inexact integration needs to be accounted for, see, for example, Ciarlet's monograph[78(§4.1)].

As already discussed, the Moulinec–Suquet discretization[4,5] arises quite naturally as a Fourier-Galerkin method with trapezoidal integration.[71] The quadrature error of the trapezoidal rule is closely linked to the error arising from trigonometric interpolation.[79] Even simpler than trigonometric interpolation is trigonometric approximation, that is, the best approximation of a given function or field by trigonometric polynomials of a given degree in an appropriate norm.[80] Therefore, it seems reasonable to understand the approximation of the solution to the cell problems first.

The difficulty is the following. Spectral methods, in particular involving trigonometric polynomials, are extremely effective for problems with smooth solutions, as trigonometric polynomials approximate such functions rapidly.[81] Much less is known for problems with discontinuous solutions like the strain field solving the cell problem with discontinuous coefficients of elasticity.

We will briefly describe the idea to leverage the theory developed for the smooth setting in the following. The impatient reader may skip these details.

Suppose we wish to estimate the following quantity $\|\boldsymbol{\varepsilon} - P_N\boldsymbol{\varepsilon}\|_{L^2}$, that is, the difference of the strain field and the trigonometric best approximation, encoded by the trigonometric projector P_N. Suppose the strain field is sufficiently smooth in the different phases of the considered multi-phase material. Moreover, assume that the strain field $\boldsymbol{\varepsilon}$ is bounded and satisfies an H^1 bound in each phase, that is, the strain gradient is square integrable. Introduce a suitable smooth cutoff function ϕ_N (see Section 2.2 for details) which is zero close to the interface and equal to unity away from the interface. Then, we may decompose the approximation error

$$\|\boldsymbol{\varepsilon} - P_N\boldsymbol{\varepsilon}\|_{L^2} \leq 2\|(1-\phi_N)\boldsymbol{\varepsilon}\|_{L^2} + \|\phi_N\boldsymbol{\varepsilon} - P_N(\phi_N\boldsymbol{\varepsilon})\|_{L^2}. \tag{1}$$

For the first term, which measures the cut-off error, we observe

$$\|(1-\phi_N)\boldsymbol{\varepsilon}\|_{L^2} \leq \|(1-\phi_N)\|_{L^2}\|\boldsymbol{\varepsilon}\|_{L^\infty} \leq C\, N^{-1/2}\|\boldsymbol{\varepsilon}\|_{L^\infty} \tag{2}$$

with a generic constant C. For the second term, by classical convergence rates for trigonometric approximation[81(Lemma 8.5.1)], we deduce

$$\begin{aligned}\|\phi_N\boldsymbol{\varepsilon} - P_N(\phi_N\boldsymbol{\varepsilon})\|_{L^2} &\leq C\,\frac{1}{N}\,\|\nabla(\phi_N\boldsymbol{\varepsilon})\|_{L^2}\\ &\leq C\,\frac{1}{N}\,(\|\nabla\phi_N\|_{L^2}\|\boldsymbol{\varepsilon}\|_{L^\infty} + \|\phi_N\,\nabla\boldsymbol{\varepsilon}\|_{L^2})\\ &\leq C\,N^{-1/2}\left(\|\boldsymbol{\varepsilon}\|_{L^\infty} + \|\boldsymbol{\varepsilon}\|_{H^1_\pm}\right)\end{aligned} \tag{3}$$

with a generic constant C that may change from line to line. Here, we used the product rule and that the term $\|\nabla\phi_N\|_{L^2}$ grows as $N^{1/2}$. Moreover, $H^1_\pm$ stands for the "broken" norm over all phases.

With the sketched argument, we showed that the strain in the Fourier-Galerkin discretization converges as $N^{-1/2}$ provided the assumed regularity assumptions on the solution of the cell problem hold (see Section 3.1 below). By the Ye–Chung argument,[73] valid for a Galerkin discretization, we thus obtain an $1/N$-convergence rate for the effective stiffness.

Even this argument for the convergence behavior of the Fourier-Galerkin discretization is not published to the best of our knowledge. However, the article at hand is more ambitious: we show an $N^{-1/2}$ convergence rate for both the local strain and stress fields in L^2 and a $1/N$ convergence rate for the effective stiffness and the Moulinec–Suquet discretization under practical assumptions on the discontinuous stiffness distribution.

Let us give a brief overview of the challenges and the strategies to overcome them. Classical convergence estimates for trigonometric interpolation[81] require sufficiently high Sobolev regularity. Indeed, these assumptions ensure Sobolev embedding into a Hölder class, $\boldsymbol{\varepsilon} \in H^k$ for $k > d/2$, where d denotes the spatial dimension, and evaluating the Fourier series pointwise makes sense. Unfortunately, the classical regularity estimates are not sufficient in the physically relevant dimensions 2 and 3, as they only provide $\boldsymbol{\varepsilon} \in H^1$ in the phases. There are more sophisticated convergence estimates for trigonometric interpolation which apply to general Riemann integrable functions.[82,83] These estimates are formulated in terms of so-called *averaged moduli of smoothness*.[79] Translated back into the scale of Sobolev spaces, we would be led to Lebesgue norms of higher mixed derivatives (up to order d in d spatial dimensions), which are known to be sharp. Thus, the basic problems remains also for these finer tools.

To overcome the problem with higher derivatives, we use *Bernstein estimates* which relate the L^p-norm of the gradient of a trigonometric polynomial to the L^p-norm of the polynomial for $1 \leq p \leq \infty$ at the expense of a prefactor that depends on the *order* of the trigonometric polynomial, see Nikol'skii[84(§2.5)] for an exposition. By a careful analysis, we are able to discard higher-order derivatives as necessary and retain only the derivatives where bounds are available in the continuous setting. Based on this strategy, we provide the desired convergence-rate estimate for the local strain and stress fields in Sections 3.3 and 3.4, respectively. Due to the interpolatory nature of the Moulinec–Suquet discretization, the convergence rate for the stresses does not immediately follow from the corresponding result of the strains, and an extra argument is required.

To provide a sharp convergence analysis of the effective stiffness, in addition to the Ye–Chung argument,[73] we must control the quadrature error. However, when inspecting the error of the trapezoidal rule, we run into essentially the same problem as for trigonometric interpolation: elementary estimates, see Section 2.3, show that mixed derivatives of high order $\partial^\alpha\boldsymbol{\varepsilon}$ for $\alpha \in \mathbb{N}^d$ with $\|\alpha\|_{\ell^\infty} = 1$ must be integrable. Using Bernstein estimates allows us to handle this case as well, see Section 3.5.

We close this section by brief remarks on organization, notation and other simplifications. Section 3 represents the core of this article, as it contains the arguments for the announced convergence rates. To increase readability, the necessary mathematical tools were out-sourced into Section 2, where characteristics of trigonometric polynomials, the delicate construction of the cut-off function and an elementary error estimate for the trapezoidal rule are collected. The sharpness of the developed theory is demonstrated via computational experiments, see Section 4.

Concerning notation, we use the $\lesssim$-symbol to replace the expression $\leq C$ with an implicit constant C to increase readability of the article. The constant depends on the spatial dimension, the lower and upper bounds (55) of the stiffness and the interface. Sometimes, we will also make the dependence on norms of the solution field $\boldsymbol{\varepsilon}$ implicit.

Last but not least, let us discuss simplifications made for the sake of exposition. We will restrict to a two-phase decomposition of the microstructure, although any finite number of phases may be treated. Also, we assume the stiffness to be

phase-wise constant, although a sufficiently smooth variation could be handled, as well. We will not take into account composite voxel methods, although they do not deteriorate the convergence rate as long as they respect the bounds on the stiffness. We will only consider cubic cells and suppose that the number of voxels N in each direction is identical. Cuboidal cells and different boxel sizes[85] in different directions can be handled at the expense of simplicity of notation and exposition.

Last but not least let us remark that we restrict to *odd* voxel numbers N to avoid discussing issues with the Nyquist frequency. This is actually only critical when bounds are desired in the Fourier-Galerkin method.[59] In practice, one may either set the Nyqvist frequency of the strain or the stress field to zero. Again, to declutter the presentation, we will omit these details.

2 | MATHEMATICAL TOOLS

2.1 | Fourier series and trigonometric polynomials

We are concerned with the cubic cell

$$\mathrm{Y}^d = [0, 2\pi]^d \tag{4}$$

in d spatial dimensions. In this manuscript N will always refer to an *odd* natural number, which controls the level of discretization. The "discrete" version of the cell (4) will be denoted as

$$\mathrm{Y}^d_N = \left\{ x_I \in \mathrm{Y}^d \;\middle|\; I \in \mathbb{Z}^d, \quad 0 \leq I_j < N, \quad j = 1, 2, \dots, d \right\}, \tag{5}$$

where the typical element x_I has the form

$$x_I = (2\pi I_1/N, 2\pi I_2/N, \dots, 2\pi I_d/N), \quad I \equiv (I_1, I_2, \dots, I_d) \in \mathbb{Z}^d. \tag{6}$$

By a trigonometric polynomial of order N on the cell Y^d we denote a function $f_N : \mathrm{Y}^d \to \mathbb{R}$ on the cell Y^d of the form

$$f_N(x) = \sum_{\xi \in \mathbb{Z}^d_N} \hat{f}_N(\xi)\, e^{ix\cdot\xi} \tag{7}$$

with suitable coefficients $\hat{f}(\xi)$ that satisfy the relations

$$\hat{f}_N(-\xi) = \overline{\hat{f}_N(\xi)}, \quad \xi \in \mathbb{Z}^d_N, \tag{8}$$

which ensure that the function f_N in the representation (7) is real-valued. To keep the notation concise, we introduced the set

$$\mathbb{Z}^d_N = \left\{ \xi \in \mathbb{Z}^d \;\middle|\; |\xi_j| < N/2, \quad j = 1, 2, \dots, d \right\} \tag{9}$$

of restricted Fourier frequencies.

We denote the (finite-dimensional) vector space of trigonometric polynomials (7) by $\mathcal{T}_N(\mathrm{Y}^d)$. In addition to scalar-valued trigonometric polynomials (7), we will frequently need vector- and tensor-valued trigonometric polynomials, as well. The statements in this section extend to trigonometric polynomials valued in a finite-dimensional Euclidean space V in a straightforward way. We denote the latter space by $\mathcal{T}_N(\mathrm{Y}^d; V)$, and will consider $V = \mathbb{R}^d$ and $V = \mathrm{Sym}(d)$, the space of symmetric $d \times d$-tensors, in this work.

Parseval's identity[86(§7)] asserts that the equality

$$⨍_{\mathrm{Y}^d} |f_N(x)|^2 \, dx = \sum_{\xi \in \mathbb{Z}^d_N} |\hat{f}_N(\xi)|^2 \tag{10}$$

holds for any trigonometric polynomial $f_N \in \mathcal{T}_N(\mathrm{Y}^d)$, where $⨍$ denotes the mean integral, that is, the integral multiplied by the inverse of the d-volume of the set. By polarization, the identity (10) also holds for the product of two trigonometric polynomials $f_N, g_N \in \mathcal{T}_N(\mathrm{Y}^d)$

$$⨍_{\mathrm{Y}^d} f_N(x) g_N(x)\, dx = \sum_{\xi \in \mathbb{Z}_N^d} \hat{f}_N(\xi) \overline{\hat{g}_N(\xi)}, \tag{11}$$

that is, the L^2 inner product between two trigonometric polynomials may either be computed by integrating in real space or by summing in Fourier space. Notice that we will always scale Lebesgue norms in such a way that mean integrals are used.

Last but not least it is also possible to describe trigonometric polynomials via interpolation. Suppose discrete values

$$\left\{ f_I \;\middle|\; I \in \mathbb{Z}^d, \quad 0 \le I_j < N \right\} \tag{12}$$

are given. Then, there is a unique polynomial $f_N \in \mathcal{T}_N(\mathrm{Y}^d)$ interpolating these values, that is, the condition

$$f_I = f_N(x_I), \quad x_I \in \mathrm{Y}_N^d, \tag{13}$$

holds for all indices I and where the points x_I are defined in Equation (5). The solution to the problem (13) is constructive and given by the discrete Fourier transform

$$\hat{f}_N(\xi) = \frac{1}{N^d} \sum_{x_I \in \mathrm{Y}_N^d} f_I\, e^{i x_I \cdot \xi}. \tag{14}$$

As a direct consequence, a discrete version of the product formula (11)

$$\frac{1}{N^d} \sum_{x_I \in \mathrm{Y}_N^d} f_N(x_I) g_N(x_I) = \sum_{\xi \in \mathbb{Z}_N^d} \hat{f}_N(\xi) \overline{\hat{g}_N(\xi)}, \quad f_N, g_N \in \mathcal{T}_N(\mathrm{Y}^d) \tag{15}$$

follows immediately. Combining the two formulas (11) and (15) yields the statement

$$⨍_{\mathrm{Y}^d} f_N(x) g_N(x)\, dx = \frac{1}{N^d} \sum_{x_I \in \mathrm{Y}_N^d} f_N(x_I) g_N(x_I), \quad f_N, g_N \in \mathcal{T}_N(\mathrm{Y}^d), \tag{16}$$

which asserts that products of trigonometric polynomials of order N may be integrated exactly by the trapezoidal rule, see Section 2.3 below.

In the article at hand, we are interested in the approximation quality of trigonometric polynomials. Any square-integrable function $f \in L^2(Y)$ admits a Fourier-series expansion[87(§4.2.4)]

$$f(x) = \sum_{\xi \in \mathbb{Z}^d} \hat{f}(\xi)\, e^{i x \cdot \xi} \tag{17}$$

to be understood in the L^2-sense. Let us denote by $P_N f$ the trigonometric polynomial

$$P_N f(x) = \sum_{\xi \in \mathbb{Z}_N^d} \hat{f}(\xi)\, e^{i x \cdot \xi} \tag{18}$$

which arises from truncating the Fourier coefficients. The trigonometric polynomial $P_N f$ represents the unique L^2-best approximation of the function f by elements of the space $\mathcal{T}_N(\mathrm{Y}^d)$ of trigonometric polynomials. The association $f \mapsto P_N f$ gives rise to a bounded linear operator P_N on the space $L^2(\mathrm{Y}^d)$ which satisfies the projector identity $P_N P_N = P_N$. A classical result of Fourier theory[87(§4.2.4)] ensures that any function f may be approximated by the trigonometric polynomial $P_N f$ in L^2, that is, the condition

$$\| f - P_N f \|_{L^2(\mathrm{Y}^d)} \to 0 \quad \text{holds as} \quad N \to \infty. \tag{19}$$

The rate of convergence may be quantified provided the function f satisfies additional regularity assumptions. More precisely, the estimate[81(Thm. 8.2.1)]

$$\|f - P_N f\|_{L^2(\mathrm{Y}^d)} \lesssim \frac{1}{N^k} \left\|\nabla^k f\right\|_{L^2(\mathrm{Y}^d)} \quad \text{holds as} \quad N \to \infty \tag{20}$$

for any $k \geq 1$ with a constant depending only on the cell Y^d, the dimension d and on the order k, provided the right-hand side is finite.

Although the trigonometric projection $P_N f$ of a given function $f \in L^2(\mathrm{Y}^d)$ is rather natural in the L^2-scale of functions, its use with other norms is rather limited. For instance, the projection $P_N f$ does not converge to the function f in the L^1-norm, in general. Also, the truncations $P_N f$ are not bounded uniformly in N for an essentially bounded function f. For this reason it is convenient to consider the Féjer approximation $F_N f \in \mathcal{T}_N(\mathrm{Y}^d)$ of a given function $f \in L^2(\mathrm{Y}^d)$, defined via the expression

$$F_N f(x) = \sum_{\xi \in \mathbb{Z}^d_N} \left(1 - \frac{|\xi_1|}{M}\right)\left(1 - \frac{|\xi_2|}{M}\right) \cdots \left(1 - \frac{|\xi_d|}{M}\right) \hat{f}(\xi)\, e^{i\, x\cdot\xi}, \quad N = 2M + 3, \tag{21}$$

see Weisz[88(§12)]. The formula (21) may be rewritten in real space in the form of a periodic convolution

$$F_N f(x) = \int_{\mathrm{Y}^d} f(x - y) K_N(y)\, dy, \quad x \in \mathrm{Y}^d, \tag{22}$$

with the non-negative and integrable kernel

$$K_N(y) = \frac{1}{M^d} \left(\frac{\sin My_1/2}{y_1/2} \frac{\sin My_2/2}{y_2/2} \cdots \frac{\sin My_d/2}{y_d/2}\right)^2 \tag{23}$$

Then, it is immediate to see that $F_N f$ converges to f in any L^p norm for $1 \leq p < \infty$ provided $f \in L^p(\mathrm{Y}^d)$.

For the manuscript at hand, we will need two properties of the Féjer means. For a start, the convolution representation (22) and Young's convolution inequality[89] imply the estimate

$$\|F_N f\|_{L^\infty(\mathrm{Y}^d)} \leq \|K_N\|_{L^1(\mathrm{Y}^d)}\ \|f\|_{L^\infty(\mathrm{Y}^d)}. \tag{24}$$

As the integral of the Féjer kernel K_N is bounded independently of N, for example, readily observed from its Fourier representation, we thus obtain that the Féjer mean $F_N f$ of a bounded function $f \in L^\infty(\mathrm{Y}^d)$ is also bounded uniformly in N, that is,

$$\|F_N f\|_{L^\infty(\mathrm{Y}^d)} \lesssim \|f\|_{L^\infty(\mathrm{Y}^d)} \tag{25}$$

holds independently of N. Moreover we take a look at the approximation quality of the Féjer means. As mentioned previously, the trigonometric projection $P_N f$ represents the L^2-best approximation to a given function f. Fortunately, the additional error introduced by using Féjer means is not too large. More precisely, the estimate

$$\|f - F_N f\|_{L^2(\mathrm{Y}^d)} \lesssim \frac{1}{N}\ \|\nabla f\|_{L^2(\mathrm{Y}^d)} \quad \text{holds as} \quad N \to \infty. \tag{26}$$

This can be seen as follows. By the triangle inequality,

$$\|f - F_N f\|_{L^2(\mathrm{Y}^d)} \leq \|f - P_N f\|_{L^2(\mathrm{Y}^d)} + \|P_N f - F_N f\|_{L^2(\mathrm{Y}^d)}, \tag{27}$$

and the estimate (20) for $k = 1$, it suffices to show

$$\|P_N f - F_N f\|_{L^2(\mathrm{Y}^d)} \lesssim \frac{1}{N}\ \|\nabla f\|_{L^2(\mathrm{Y}^d)}. \tag{28}$$

By Parseval's identity (10) and the definition (21) of the Féjer means, we observe

$$\|P_N f - F_N f\|^2_{L^2(\mathrm{Y}^d)} = \sum_{\xi\in\mathbb{Z}^d_N} \left(\left(1 - \frac{|\xi_1|}{M}\right)\left(1 - \frac{|\xi_2|}{M}\right)\cdots\left(1 - \frac{|\xi_d|}{M}\right) - 1 \right)^2 \left|\hat{f}(\xi)\right|^2 \tag{29}$$

The term in squares is given as a sum of products of the form $|\xi^\alpha|/M^{|\alpha|}$ for multi-indices $\alpha \in \mathbb{N}^d$ whose components are not all equal to zero. Using the estimate $|\xi_i| \leq M$ implied by the definition of the set $\mathbb{Z}^d_N$, see Equation (9), we are led to the bound

$$\|P_N f - F_N f\|^2_{L^2(\mathrm{Y}^d)} \lesssim \sum_{\xi\in\mathbb{Z}^d_N} \left(\frac{|\xi_1|}{M} + \frac{|\xi_2|}{M} + \ldots + \frac{|\xi_d|}{M} \right)^2 \left|\hat{f}(\xi)\right|^2 \tag{30}$$

with a constant depending only on the dimension d, which readily implies the statement (28), whose validity implies the convergence rate assertion (26).

We will conclude this section with two further results about trigonometric polynomials. The first concerns convergence rates of trigonometric interpolation. For a given bounded function f, denote by $Q_N[f] \in \mathcal{T}_N(\mathrm{Y}^d)$ the unique trigonometric polynomial f_N which satisfies the interpolation conditions (13) for $f_I \equiv f(x_I), x_I \in \mathrm{Y}^d_N$. Trigonometric interpolation is more subtle than trigonometric approximation as the former is not well-defined on Lebesgue spaces. Indeed, for interpolation to be reasonable, the function values to be interpolated need to be finite. Moreover, Fourier series need not converge pointwise, and arguments based on Fourier series may not be applicable. These problems may be overcome provided the function to be interpolated is sufficiently smooth. Indeed, Hölder continuity is a sufficient condition for a Fourier series to converge pointwise, and Hölder continuity is in turn implied by Sobolev embedding provided the sufficiently high derivatives of the function under consideration belong to suitable Lebesgue spaces. Then, the following result

$$\|f - Q_N[f]\|_{L^2(\mathrm{Y}^d)} \lesssim \frac{1}{N^k} \left\|\nabla^k f\right\|_{L^2(\mathrm{Y}^d)} \quad \text{holds as} \quad N \to \infty \tag{31}$$

may be shown, see, for example, Vondřejc et al.[71(Lemma 4)], where the index k satisfies the condition $k > d/2$ required for the Sobolev embedding theorem[90(Ch.V, Thm. 2(iii))] to hold. Thus, the convergence rate of trigonometric interpolation (31) coincides with the rate of trigonometric approximation (20), at least for sufficiently regular functions.

Unfortunately, the regularity of the solutions to the micromechanical problems considered in this article is not sufficient to ensure the interpolation estimate (31) to hold. Therefore, it is convenient to use *inverse estimates* to trade (higher-order) derivatives for powers of the discretization parameter N. Of course, such a strategy is only feasible on a suitable finite-dimensional space of functions like the space of trigonometric polynomials. The prototypical result which we need is the following Bernstein estimate

$$\|\partial^\alpha f_N\|_{L^\infty(\mathrm{Y}^d)} \lesssim N^{|\alpha|} \, \|f_N\|_{L^\infty(\mathrm{Y}^d)}, \tag{32}$$

valid for any $f_N \in \mathcal{T}_N(\mathrm{Y}^d)$ and multi-index $\alpha \in \mathbb{N}^d$. In particular, for any trigonometric polynomial $f_N \in \mathcal{T}_N(\mathrm{Y}^d)$, the derivative $\partial_j f_N$ does not exceed $N\|f_N\|_{L^\infty(\mathrm{Y}^d)}$ up to a constant depending only on the dimension d and the cell Y^d.

The classical Bernstein estimate

$$\|f_N'\|_{L^\infty([0,2\pi])} \lesssim N \, \|f_N\|_{L^\infty([0,2\pi])} \tag{33}$$

concerns one-dimensional trigonometric polynomials $f_N \in \mathcal{T}_1([0, 2\pi])$, see Nikol'skii[84(§2.5)] for a proof. Applying this estimate to a single coordinate $j \in \{1, 2, \ldots, d\}$ and noticing that the function $x_j \mapsto f_N(x_1, \ldots, x_{j-1}, x_j, x_{j+1}, \ldots, x_d)$ is a one-dimensional trigonometric polynomial of order N leads to the estimate

$$\left\|\partial_j f_N\right\|_{L^\infty(\mathrm{Y}^d)} \lesssim N \, \|f_N\|_{L^\infty(\mathrm{Y}^d)}, \tag{34}$$

which implies the general assertion (32) by treating a single derivative at a time.

We will also need the L^2-version of the Bernstein estimate (32) in L^∞

$$\|\partial^\alpha f_N\|_{L^2(\mathrm{Y}^d)} \lesssim N^{|\alpha|} \, \|f_N\|_{L^2(\mathrm{Y}^d)}, \tag{35}$$

valid for any $f_N \in \mathcal{T}_N(\mathrm{Y}^d)$ and multi-index $\alpha \in \mathbb{N}^d$. The estimate (35) follows from the formula

$$\widehat{\partial^\alpha f}(\xi) = i^{|\alpha|}\xi^\alpha \hat{f}(\xi) \tag{36}$$

for the Fourier coefficients of derivatives, Parseval's identity (11) and the fact that the nonzero frequencies of a trigonometric polynomial (7) are concentrated in the set $\mathbb{Z}^d_N$, see Equation (9), s.t., $|\xi_j| \leq N/2$ holds.

2.2 | Cutting off smoothly at the interface

We are interested in composite materials, that is, those whose microstructure consists of a number of distinct materials, for example, a matrix-inclusion composite. Due to the different material behavior in the phases, the mechanical fields are not smooth across the interfaces. Rather, the solutions to the governing equations are only contained in *broken* Sobolev spaces. To make this precise, we suppose that the microstructure Y^d admits the non-overlapping decomposition

$$\mathrm{Y}^d = \overline{\mathrm{Y}^d_+} \cup \overline{\mathrm{Y}^d_-}, \quad \mathrm{Y}^d_+ \cap \mathrm{Y}^d_- = \emptyset, \tag{37}$$

into two open subsets $\mathrm{Y}^d_\pm$ whose boundary $\partial\mathrm{Y}^d_\pm$, considered as a Y^d-periodic object, is sufficiently smooth. More precisely, the interface should be in the Hölder class $C^{1,\alpha}$ for positive α for the Li–Nirenberg estimates[91] to hold.

For the subsequent discussion, let

$$\delta : \mathrm{Y}^d \to \mathbb{R}_{\geq 0} \tag{38}$$

denote the periodic distance to the interface $\partial\mathrm{Y}^d_\pm$. The distance function (38) is continuous. Moreover, due to the smoothness of the interface, the distance function δ is also smooth in the vicinity of the interface, that is, there is a natural number N_0, s.t. the function δ is sufficiently smooth at all points $x \in \mathrm{Y}^d$ which are $1/(2N_0)$-close to the interface, that is, which satisfy $\delta(x) \leq 1/(2N_0)$. We will tacitly assume the condition $N \geq N_0$ to hold in the subsequent manuscript.

For the following construction we fix a smooth, that is, infinitely often continuously differentiable, function $\eta : \mathbb{R}_{\geq 0} \to [0,1]$, s.t. the conditions

$$\eta(x) = 0, \quad x \leq 1, \quad \text{and} \quad \eta(x) = 1, \quad x \geq 2 \tag{39}$$

hold. Such a function is easily constructed, for example, by mollifying a piece-wise linear function. We fix once and for all such a function η, satisfying the conditions (39). Properties of the function, in particular upper bounds on the partial derivatives, will enter our estimates as *universal constants*.

With the function η at hand, we define the cutoff function

$$\phi_N : \mathrm{Y}^d \to \mathbb{R}_{\geq 0} \quad \text{by} \quad \phi_N(x) = \eta\left(\frac{\delta(x)}{N}\right), \tag{40}$$

where N is a positive integer. For sufficiently large parameter N, the function ϕ_N is smooth and permits to patch together a function $f : \mathrm{Y}^d \to \mathbb{R}$ whose restrictions $f_\pm : \mathrm{Y}^d_\pm \to \mathbb{R}$ are smooth to a smooth function on the entire cell. More precisely, the function $\phi_N f$ coincides with the original function f for points x whose distance to the interface exceeds $2/N$. $1/N$-close to the interface, the function $\phi_N f$ vanishes identically.

In the remainder of the section, we quantify the error introduced by this smoothing procedure in Sobolev norms. By construction (39) of the function η, the function ϕ_N satisfies the bound

$$\|\phi_N\|_{L^\infty} \leq 1, \quad N \in \mathbb{N}. \tag{41}$$

Moreover, the function ϕ_N satisfies the condition

$$\nabla\phi_N(x) = 0 \quad \text{for} \quad \delta(x) \leq \frac{1}{N} \quad \text{as well as} \quad \delta(x) \geq \frac{2}{N} \tag{42}$$

and the estimate

$$\left\|\nabla^k \phi_N(x)\right\| \lesssim N^k \quad \text{for} \quad \frac{1}{N} < \delta(x) < \frac{2}{N} \tag{43}$$

with a constant that depends on the interface, the dimension and the function η. In particular, for any multi-index $\alpha \in \mathbb{N}^d \setminus \{0\}$ and every exponent $p \in [1, \infty)$, we obtain the estimate

$$\begin{aligned} \|\partial^\alpha \phi_N\|_{L^p(\mathrm{Y}^d)}^p &= \fint_{\mathrm{Y}^d} \|\partial^\alpha \phi_N(x)\|^p \, dx \\ &\lesssim \int_{1<N\delta(x)<2} N^{|\alpha|p} \, dx \\ &\lesssim N^{|\alpha|p-1}, \end{aligned} \tag{44}$$

which implies the bound

$$\|\partial^\alpha \phi_N\|_{L^p(\mathrm{Y}^d)} \lesssim N^{|\alpha|-1/p}. \tag{45}$$

Notable special cases include

$$\|\nabla \phi_N\|_{L^1(\mathrm{Y}^d)} \lesssim 1 \quad \text{and} \quad \|\nabla \phi_N\|_{L^2(\mathrm{Y}^d)} \lesssim N^{1/2}. \tag{46}$$

We will also need the elementary estimate

$$\|1 - \phi_N\|_{L^p(\mathrm{Y}^d)} \lesssim N^{-\frac{1}{p}}. \tag{47}$$

2.3 | The trapezoidal rule for rough functions

The Moulinec–Suquet discretization[4,5] was identified as a Fourier-Galerkin discretization with numerical integration by Vondřejc et al.[71] More precisely, the trapezoidal rule (apparently in use since more than 2000 years[92]) was used as the quadrature rule in question.

The trapezoidal rule is rather simple, but turns out to be quite powerful for smooth periodic functions.[93] In one spatial dimension, the classical analysis of the trapezoidal rule shows that using N integration points leads to an error which decays as N^{-2} with a constant that involves the maximum of the second derivative of the function to be integrated[94(eq.(5.1.7))]. For the manuscript at hand, the L^∞-norm is not suitable, see Section 2.2, and estimates in Lebesgue norms are required. Our subsequent discussion is based on the following one-dimensional result, which may be used to analyze the convergence behavior of the trapezoidal rule of rather rough functions, see Cruz-Uribe and Neugebauer.[95]

For any positive integer $N \in \mathbb{N}$ there is a function $w_N : [0, 2\pi] \to \mathbb{R}$, bounded uniformly in N, s.t., for any continuous and periodic function $f : [0, 2\pi] \to \mathbb{R}$ with integrable weak derivative f' the representation

$$\frac{1}{N} \sum_{j=1}^{N} f\left(\frac{2\pi j}{N}\right) = \fint_0^{2\pi} f(x) \, dx + \frac{1}{N} \fint_0^{2\pi} f'(x) \, w_N(x) \, dx \tag{48}$$

holds, where $\fint$ refers to the mean integral.

The result in well known. For the reader's convenience, a derivation is included in Appendix A.

In one dimension, equation (48) can be used to bound the error decay for the trapezoidal rule

$$\left| \fint_0^{2\pi} f(x) \, dx - \frac{1}{N} \sum_{j=1}^{N} f\left(\frac{2\pi j}{N}\right) \right| \lesssim \frac{1}{N} \, \|f'\|_{L^1} \tag{49}$$

with a constant independent of the function f and the parameter N.

Applying the representation formula (48) for each dimension individually, we arrive at an estimate for the error of the trapezoidal rule in d dimensions.

For any dimension $d \in \mathbb{N}$, there is a constant C, s.t. for any continuous periodic function $f : [0, 2\pi]^d \to \mathbb{R}$ whose derivatives are integrable up to order d, the estimate

$$\left| \fint_{\mathrm{Y}^d} f(x) \, dx - \frac{1}{N^d} \sum_{x_I \in \mathrm{Y}_N^d} f(x_I) \right| \lesssim \sum_{\|\alpha\|_\infty = 1} \frac{1}{N^{|\alpha|}} \, \|\partial^\alpha f\|_{L^1(\mathrm{Y}^d)} \tag{50}$$

holds, where $\alpha = (\alpha_1, \dots, \alpha_d) \in \mathbb{N}^d$ is a multi-index with

$$\partial^\alpha f \equiv \frac{\partial^{|\alpha|} f}{\partial_1^{\alpha_1} \cdots \partial_d^{\alpha_d}} \quad \text{and} \quad |\alpha| \equiv \|\alpha\|_1. \tag{51}$$

Indeed, applying the identity (48) for each dimension individually we arrive at the representation

$$\frac{1}{N^d} \sum_{x_I \in \mathrm{Y}_N^d} f(x_I) = \fint_{[0,2\pi]^d} f(x)\, dx + \sum_{\|\alpha\|_\infty = 1} \frac{1}{N^{|\alpha|}} \fint_{[0,2\pi]^d} \partial^\alpha f(x) w_N^\alpha(x)\, dx, \tag{52}$$

see Verlinden et al.[96(§5)], with the short-hand notation

$$w_N^\alpha(x) = w_N(x_1)^{\alpha_1} \cdots w_N(x_d)^{\alpha_d}. \tag{53}$$

Due to the boundedness of the weight function w_N, uniformly in N, the estimate (50) follows from a repeated application of the triangle inequality and Hölder's inequality in view of the N-independent bound on the functions w_N.

Apart from the gradient of the function f, the estimate (50) involves *mixed* derivatives up to the order of the dimension, for example, the quantity $\partial_1 \partial_2 \partial_3 f$ in dimension $d = 3$.

3 | CONVERGENCE OF THE MOULINEC–SUQUET DISCRETIZATION

3.1 | The homogenization problem

Suppose that the microstructure Y^d is decomposed according to equation (37) with a sufficiently smooth interface s.t. the constructions of Section 2.2 are valid. Let stiffness tensors $\mathbb{C}_\pm$ be given, that is, linear operators on the space $\mathrm{Sym}(d)$ of symmetric $d \times d$-tensors, which are symmetric in the sense that

$$\boldsymbol{\varepsilon}_1 : \mathbb{C}_\pm : \boldsymbol{\varepsilon}_2 = \boldsymbol{\varepsilon}_2 : \mathbb{C}_\pm : \boldsymbol{\varepsilon}_1 \quad \text{holds for} \quad \boldsymbol{\varepsilon}_j \in \mathrm{Sym}(d), \quad j = 1, 2, \tag{54}$$

with the double-contraction operator defined by $\boldsymbol{\varepsilon}_1 : \boldsymbol{\varepsilon}_2 = \mathrm{tr}(\boldsymbol{\varepsilon}_1 \boldsymbol{\varepsilon}_2)$, and positive definite. Denote by $\underline{\alpha}$ and $\overline{\alpha}$ positive constants, s.t. the estimates

$$\underline{\alpha}\, \|\boldsymbol{\varepsilon}\|^2 \le \boldsymbol{\varepsilon} : \mathbb{C}_\pm : \boldsymbol{\varepsilon} \le \overline{\alpha}\, \|\boldsymbol{\varepsilon}\|^2, \quad \boldsymbol{\varepsilon} \in \mathrm{Sym}(d), \tag{55}$$

hold for both $\mathbb{C}_+$ and $\mathbb{C}_-$ in terms of the norm $\|\boldsymbol{\varepsilon}\| = (\boldsymbol{\varepsilon} : \boldsymbol{\varepsilon})^{1/2}$. Define the heterogeneous stiffness field $\mathbb{C} : \mathrm{Y}^d \to L(\mathrm{Sym}(d))$ via

$$\mathbb{C}(x) = \begin{cases} \mathbb{C}_-, & x \in \overline{\mathrm{Y}_-^d}, \\ \mathbb{C}_+, & x \in \mathrm{Y}_+^d. \end{cases} \tag{56}$$

For prescribed macroscopic strain $\overline{\boldsymbol{\varepsilon}} \in \mathrm{Sym}(d)$, we seek the periodic displacement field $\boldsymbol{u} \in H^1_\#(\mathrm{Y}^d; \mathbb{R}^d)$, the closure of smooth periodic and mean-free fields on the periodic cell Y^d w.r.t. the H^1-norm, solving the equation

$$\left\langle \nabla^s \boldsymbol{v} : \mathbb{C} : (\overline{\boldsymbol{\varepsilon}} + \nabla^s \boldsymbol{u}) \right\rangle_Y = 0 \quad \text{for all} \quad \boldsymbol{v} \in H^1_\#(\mathrm{Y}^d; \mathbb{R}^d), \tag{57}$$

where ∇^s refers to the symmetrized gradient and the operator $\langle \cdot \rangle_Y$ is a short-hand notation for the mean integral over the unit cell Y^d.

Based on the inequalities of Korn and Poincaré, the Riesz representation theorem is readily applied to show existence and uniqueness of solutions to the problem (57).

Li and Nirenberg[91] showed that the solution $\boldsymbol{u}$ to the problem (57) has a uniformly bounded strain, that is, the estimate

$$\|\boldsymbol{\varepsilon}\|_{L^\infty(\mathrm{Y}^d)} \lesssim 1 \quad \text{holds for} \quad \boldsymbol{\varepsilon} = \overline{\boldsymbol{\varepsilon}} + \nabla^s \boldsymbol{u} \tag{58}$$

and the restriction of the displacement fluctuation field $\boldsymbol{u}$ to the sets $\mathrm{Y}^d_\pm$ lies in the Sobolev space H^2, that is, the inequalities

$$\|\boldsymbol{\varepsilon}\|_{H^1(\mathrm{Y}^d_\pm)} \lesssim 1 \quad \text{are valid for} \quad \boldsymbol{\varepsilon} = \overline{\boldsymbol{\varepsilon}} + \nabla^s \boldsymbol{u} \tag{59}$$

on the decomposing domains $\mathrm{Y}^d_\pm$. The two higher regularity estimates (58) and (59) will be used to derive convergence estimates for the Moulinec–Suquet discretization. We are not aware of similar results beyond the linear (thermo-)elastic setting, which is why we restrict to this setting. Indeed, a-priori estimates and convergence results (without explicit rates) are available for the more general setting of strongly monotone and Lipschitz continuous stress operators.[57] Higher regularity results are lacking, compare for instance Neff and Knees[97] for work in this direction (treating boundary regularity instead of interface regularity).

Let us emphasize the dependence of the solution $\boldsymbol{u}$ on the macroscopic strain $\overline{\boldsymbol{\varepsilon}}$ by a subindex, that is, we write $\boldsymbol{u}_{\overline{\boldsymbol{\varepsilon}}}$. Then, the effective stiffness $\mathbb{C}^{\mathtt{eff}} \in L(\mathrm{Sym}(d))$ of the microscopic stiffness distribution $\mathbb{C}$ is defined by

$$\mathbb{C}^{\mathtt{eff}} : \overline{\boldsymbol{\varepsilon}} = \left\langle \mathbb{C} : \left(\overline{\boldsymbol{\varepsilon}} + \nabla^s \boldsymbol{u}_{\overline{\boldsymbol{\varepsilon}}}\right) \right\rangle_Y. \tag{60}$$

Showing that this construction is well-defined and gives rise to a symmetric stiffness respecting the bounds (55) is standard, see, for example, the arguments in Schneider[72(Corollary 2.2)]. For our purposes, we need the representation formula

$$\overline{\boldsymbol{\varepsilon}}_1 : \mathbb{C}^{\mathtt{eff}} : \overline{\boldsymbol{\varepsilon}}_2 = \left\langle \left(\overline{\boldsymbol{\varepsilon}}_1 + \nabla^s \boldsymbol{u}_{\overline{\boldsymbol{\varepsilon}}_1}\right) : \mathbb{C} : \left(\overline{\boldsymbol{\varepsilon}}_2 + \nabla^s \boldsymbol{u}_{\overline{\boldsymbol{\varepsilon}}_2}\right) \right\rangle_Y, \quad \boldsymbol{\varepsilon}_1, \boldsymbol{\varepsilon}_2 \in \mathrm{Sym}(d), \tag{61}$$

which is a direct consequence of the validity of the cell problem (57) and the definition (60).

3.2 | The a-priori estimate

For any odd positive integer N, the Moulinec–Suquet discretization[4,5] seeks a displacement field $\boldsymbol{u}_N \in \mathcal{T}_N(\mathrm{Y}^d; \mathbb{R}^d)$, s.t. the equation

$$\frac{1}{N^d} \sum_{x_I \in \mathrm{Y}^d_N} \nabla^s \boldsymbol{v}_N(x_I) : \mathbb{C}(x_I) : (\overline{\boldsymbol{\varepsilon}} + \nabla^s \boldsymbol{u}_N(x_N)) = 0 \tag{62}$$

is satisfied for all test fields $\boldsymbol{v}_N \in \mathcal{T}_N(\mathrm{Y}^d; \mathbb{R}^d)$. As observed by Vondřjec et al.,[71] the Moulinec–Suquet discretization proceeds by restricting the space of ansatz and test fields to trigonometric polynomials and replaces the integrals appearing in the cell problem (57) by the trapezoidal rule.

For the analysis, it is convenient to recast the Equation (62) in terms of the trigonometric interpolation operator Q_N.[71,72] Indeed, due to Parseval's identity (11), Equation (62) may be rewritten in the form

$$\left\langle \nabla^s \boldsymbol{v}_N : Q_N \left[\mathbb{C} : (\overline{\boldsymbol{\varepsilon}} + \nabla^s \boldsymbol{u}_N)\right] \right\rangle_Y = 0 \quad \text{for all} \quad \boldsymbol{v}_N \in \mathcal{T}_N(\mathrm{Y}^d; \mathbb{R}^d). \tag{63}$$

Introducing the stress field $\boldsymbol{\sigma}_N \equiv Q_N \left[\mathbb{C} : (\overline{\boldsymbol{\varepsilon}} + \nabla^s \boldsymbol{u}_N)\right] \in \mathcal{T}_N(\mathrm{Y}^d; \mathrm{Sym}(d))$, the equation (63) is, in turn, equivalent to the strong form

$$\mathrm{div}\ \sigma_N = 0 \tag{64}$$

of the quasi-static balance of linear momentum. This property contrasts with traditional finite element discretizations, where both the compatibility and the material law are evaluated exactly, but the equilibrium equation (64) is approximated. Indeed, the Moulinec–Suquet discretization works with a compatible strain field $\boldsymbol{\varepsilon}_N = \overline{\boldsymbol{\varepsilon}} + \nabla^s \boldsymbol{u}_N \in \mathcal{T}_N(\mathrm{Y}^d; \mathrm{Sym}(d))$ and a self-equilibrated stress field $\boldsymbol{\sigma}_N \in \mathcal{T}_N(\mathrm{Y}^d; \mathrm{Sym}(d))$, but the constitutive law

$$\boldsymbol{\sigma}_N(x_I) = \mathbb{C}(x_I) : \boldsymbol{\varepsilon}_N(x_I), \quad x_I \in \mathrm{Y}^d_N \tag{65}$$

is valid only in the collocation (or quadrature) points.

Under the hypothesis (55), the equation (62) admits a unique solution $\boldsymbol{u}_N$ among the trigonometric polynomials $\mathcal{T}_N(\mathrm{Y}^d; \mathbb{R}^d)$ with vanishing mean. This can be seen as follows.[71] Writing the problem (62) in the suggestive form

$$\frac{1}{N^d}\sum_{x_I\in \mathrm{Y}_N^d} \nabla^s \boldsymbol{v}_N(x_I) : \mathbb{C}(x_I) : \nabla^s \boldsymbol{u}_N(x_N) = -\frac{1}{N^d}\sum_{x_I\in \mathrm{Y}_N^d} \nabla^s \boldsymbol{v}_N(x_I) : \mathbb{C}(x_I) : \overline{\boldsymbol{\varepsilon}}, \tag{66}$$

existence and uniqueness follows from the Riesz representation theorem[87(Thm.4.17)]. Indeed, the right-hand side is apparently linear in the test field, whereas the left-hand side represents a symmetric bilinear form in the fields $\boldsymbol{u}_N$ and $\boldsymbol{v}_N$, respectively. Due to the bound (55), we may estimate

$$\begin{aligned}\frac{1}{N^d}\sum_{x_I\in \mathrm{Y}_N^d} \nabla^s \boldsymbol{u}_N(x_I) : \mathbb{C}(x_I) : \nabla^s \boldsymbol{u}_N(x_N) &\geq \underline{\alpha}\, \frac{1}{N^d}\sum_{x_I\in \mathrm{Y}_N^d} \|\nabla^s \boldsymbol{u}_N(x_I)\|^2 \\ &= \underline{\alpha}\, \left\langle \|\nabla^s \boldsymbol{u}_N\|^2 \right\rangle_Y \\ &\gtrsim \underline{\alpha}\, \left\langle \|\nabla \boldsymbol{u}_N\|^2 \right\rangle_Y \\ &\gtrsim \underline{\alpha}\, \left\langle \|\boldsymbol{u}_N - \langle \boldsymbol{u}_N\rangle_Y\|^2 \right\rangle_Y\end{aligned} \tag{67}$$

where we used Parseval's identity, Korn's inequality[98] and Poincaré's inequality[99(§5.8.1)] on the flat torus.

After recalling the argument[71] for existence and uniqueness of solutions to the discretized cell problem (62), we provide a stream-lined argument for a-priori estimate[71(Proof of Prop.8)] which is essential for the analysis in Section 3.3. Denote by $\boldsymbol{\varepsilon}_N = \overline{\boldsymbol{\varepsilon}} + \nabla^s \boldsymbol{u}_N$ the strain associated to the solution $\boldsymbol{u}_N$ of the cell problem (62) in response to the imposed strain $\overline{\boldsymbol{\varepsilon}} \in \mathrm{Sym}(d)$. We denote by

$$\tilde{\boldsymbol{\varepsilon}}_N = \overline{\boldsymbol{\varepsilon}} + \nabla^s \boldsymbol{w}_N, \quad \boldsymbol{w}_N \in \mathcal{T}_N(\mathrm{Y}^d;\mathbb{R}^d), \tag{68}$$

any compatible competition strain. Then, the difference between these two strains admits the representation

$$\boldsymbol{\varepsilon}_N - \tilde{\boldsymbol{\varepsilon}}_N = \nabla^s \boldsymbol{v}_N \quad \text{with} \quad \boldsymbol{v}_N \equiv \boldsymbol{u}_N - \boldsymbol{w}_N \in \mathcal{T}_N(\mathrm{Y}^d;\mathbb{R}^d). \tag{69}$$

In particular, we observe

$$\begin{aligned}\underline{\alpha}\, \|\boldsymbol{\varepsilon}_N - \tilde{\boldsymbol{\varepsilon}}_N\|^2_{L^2(\mathrm{Y}^d)} &\leq \left\langle (\boldsymbol{\varepsilon}_N - \tilde{\boldsymbol{\varepsilon}}_N) : Q_N\left[\mathbb{C} : (\boldsymbol{\varepsilon}_N - \tilde{\boldsymbol{\varepsilon}}_N)\right]\right\rangle_Y \\ &= \left\langle (\boldsymbol{\varepsilon}_N - \tilde{\boldsymbol{\varepsilon}}_N) : Q_N\left[\mathbb{C} : \boldsymbol{\varepsilon}_N\right]\right\rangle_Y - \left\langle (\boldsymbol{\varepsilon}_N - \tilde{\boldsymbol{\varepsilon}}_N) : Q_N\left[\mathbb{C} : \tilde{\boldsymbol{\varepsilon}}_N\right]\right\rangle_Y \\ &= \left\langle \nabla^s \boldsymbol{v}_N : Q_N\left[\mathbb{C} : \boldsymbol{\varepsilon}_N\right]\right\rangle_Y - \left\langle (\boldsymbol{\varepsilon}_N - \tilde{\boldsymbol{\varepsilon}}_N) : Q_N\left[\mathbb{C} : \tilde{\boldsymbol{\varepsilon}}_N\right]\right\rangle_Y \\ &= -\left\langle (\boldsymbol{\varepsilon}_N - \tilde{\boldsymbol{\varepsilon}}_N) : Q_N\left[\mathbb{C} : \tilde{\boldsymbol{\varepsilon}}_N\right]\right\rangle_Y\end{aligned} \tag{70}$$

in view of the discretized cell problem (63). Arguing in a reverse order but using the continuous cell problem (57) yields the chain of arguments

$$\begin{aligned}\underline{\alpha}\|\boldsymbol{\varepsilon}_N - \tilde{\boldsymbol{\varepsilon}}_N\|^2_{L^2(\mathrm{Y}^d)} &\leq -\left\langle (\boldsymbol{\varepsilon}_N - \tilde{\boldsymbol{\varepsilon}}_N) : Q_N\left[\mathbb{C} : \tilde{\boldsymbol{\varepsilon}}_N\right]\right\rangle_Y \\ &= \langle \nabla^s \boldsymbol{v}_N : \mathbb{C} : \boldsymbol{\varepsilon}\rangle_Y - \left\langle (\boldsymbol{\varepsilon}_N - \tilde{\boldsymbol{\varepsilon}}_N) : Q_N\left[\mathbb{C} : \tilde{\boldsymbol{\varepsilon}}_N\right]\right\rangle_Y \\ &= \langle (\boldsymbol{\varepsilon}_N - \tilde{\boldsymbol{\varepsilon}}_N) : \mathbb{C} : \boldsymbol{\varepsilon}\rangle_Y - \left\langle (\boldsymbol{\varepsilon}_N - \tilde{\boldsymbol{\varepsilon}}_N) : Q_N\left[\mathbb{C} : \tilde{\boldsymbol{\varepsilon}}_N\right]\right\rangle_Y \\ &= \left\langle (\boldsymbol{\varepsilon}_N - \tilde{\boldsymbol{\varepsilon}}_N) : \left(\mathbb{C} : \boldsymbol{\varepsilon} - Q_N\left[\mathbb{C} : \tilde{\boldsymbol{\varepsilon}}_N\right]\right)\right\rangle_Y.\end{aligned} \tag{71}$$

Applying the Cauchy-Schwarz inequality yields the desired a-priori estimate

$$\|\boldsymbol{\varepsilon}_N - \tilde{\boldsymbol{\varepsilon}}_N\|_{L^2(\mathrm{Y}^d)} \leq \frac{1}{\underline{\alpha}}\, \left\|\mathbb{C} : \boldsymbol{\varepsilon} - Q_N\left[\mathbb{C} : \tilde{\boldsymbol{\varepsilon}}_N\right]\right\|_{L^2(\mathrm{Y}^d)}. \tag{72}$$

This inequality served as the basis of previous convergence proofs[71-73] which either required higher regularity of the solution field $\boldsymbol{u}$ or led to convergence results without explicit rates. The mentioned strategies selected

$$\tilde{\boldsymbol{\varepsilon}}_N = P_N \boldsymbol{\varepsilon} \quad \text{with} \quad \boldsymbol{\varepsilon} = \overline{\boldsymbol{\varepsilon}} + \nabla^s \boldsymbol{u}, \quad \text{that is,} \quad \tilde{\boldsymbol{\varepsilon}}_N = \overline{\boldsymbol{\varepsilon}} + \nabla^s P_N \boldsymbol{u} \tag{73}$$

in terms of the trigonometric approximation operator (18).

3.3 | Convergence rate for the strain field

The goal of this section is to show the convergence-rate estimate

$$\|\boldsymbol{\varepsilon} - \boldsymbol{\varepsilon}_N\|_{L^2(\mathrm{Y}^d)} \lesssim N^{-\frac{1}{2}} \tag{74}$$

for the strain field in the Moulinec–Suquet discretization, where the constant depends on the dimension, the interface, the ellipticity ratio, the L^∞-bound on the strain field $\boldsymbol{\varepsilon}$ and the H^1-bounds on the strain field $\boldsymbol{\varepsilon}$ on the subdomains $\mathrm{Y}^d_\pm$.

To analyze the convergence behavior of the strain field, our strategy utilizes Féjer means (21) instead of the trigonometric projection (18). More precisely, instead of equation (73), we set

$$\tilde{\boldsymbol{\varepsilon}}_N = F_N \boldsymbol{\varepsilon} \quad \text{with} \quad \boldsymbol{\varepsilon} = \overline{\boldsymbol{\varepsilon}} + \nabla^s \boldsymbol{u}, \quad \text{that is,} \quad \tilde{\boldsymbol{\varepsilon}}_N = \overline{\boldsymbol{\varepsilon}} + \nabla^s F_N \boldsymbol{u}. \tag{75}$$

By the triangle inequality and the a-priori estimate (72), we deduce

$$\begin{aligned} \|\boldsymbol{\varepsilon} - \boldsymbol{\varepsilon}_N\|_{L^2(\mathrm{Y}^d)} &\leq \|\boldsymbol{\varepsilon} - \tilde{\boldsymbol{\varepsilon}}_N\|_{L^2(\mathrm{Y}^d)} + \|\boldsymbol{\varepsilon}_N - \tilde{\boldsymbol{\varepsilon}}_N\|_{L^2(\mathrm{Y}^d)} \\ &\leq \|\boldsymbol{\varepsilon} - \tilde{\boldsymbol{\varepsilon}}_N\|_{L^2(\mathrm{Y}^d)} + \frac{1}{\underline{\alpha}} \left\| \mathbb{C} : \boldsymbol{\varepsilon} - Q_N \left[\mathbb{C} : \tilde{\boldsymbol{\varepsilon}}_N \right] \right\|_{L^2(\mathrm{Y}^d)} \\ &\leq \left(1 + \frac{\overline{\alpha}}{\underline{\alpha}} \right) \|\boldsymbol{\varepsilon} - \tilde{\boldsymbol{\varepsilon}}_N\|_{L^2(\mathrm{Y}^d)} + \frac{1}{\underline{\alpha}} \left\| \mathbb{C} : \tilde{\boldsymbol{\varepsilon}}_N - Q_N \left[\mathbb{C} : \tilde{\boldsymbol{\varepsilon}}_N \right] \right\|_{L^2(\mathrm{Y}^d)}. \end{aligned} \tag{76}$$

Thus, the discretization error is naturally split into an *approximation* error

$$\|\boldsymbol{\varepsilon} - \tilde{\boldsymbol{\varepsilon}}_N\|_{L^2(\mathrm{Y}^d)} \equiv \|\boldsymbol{\varepsilon} - F_N \boldsymbol{\varepsilon}\|_{L^2(\mathrm{Y}^d)} \tag{77}$$

and an *interpolation* error

$$\left\| \mathbb{C} : \tilde{\boldsymbol{\varepsilon}}_N - Q_N \left[\mathbb{C} : \tilde{\boldsymbol{\varepsilon}}_N \right] \right\|_{L^2(\mathrm{Y}^d)} \equiv \left\| \mathbb{C} : F_N \boldsymbol{\varepsilon} - Q_N \left[\mathbb{C} : F_N \boldsymbol{\varepsilon} \right] \right\|_{L^2(\mathrm{Y}^d)}. \tag{78}$$

Thus, to derive convergence rates for the discretization error, we analyze these two contributions individually. For the approximation error (77), we would like to apply classical convergence rate estimates for trigonometric approximation (20). However, the strain field $\boldsymbol{\varepsilon}$ lacks the necessary regularity, and we rely upon the smoothing approach introduced in Section 2.2. We write

$$\begin{aligned} \|\boldsymbol{\varepsilon} - F_N \boldsymbol{\varepsilon}\|_{L^2(\mathrm{Y}^d)} &\leq \|(1 - \phi_N)\boldsymbol{\varepsilon}\|_{L^2(\mathrm{Y}^d)} + \|\phi_N \boldsymbol{\varepsilon} - F_N[\phi_N \boldsymbol{\varepsilon}]\|_{L^2(\mathrm{Y}^d)} + \|F_N \left[(1 - \phi_N)\boldsymbol{\varepsilon} \right]\|_{L^2(\mathrm{Y}^d)} \\ &\leq 2\|(1 - \phi_N)\boldsymbol{\varepsilon}\|_{L^2(\mathrm{Y}^d)} + \|\phi_N \boldsymbol{\varepsilon} - F_N[\phi_N \boldsymbol{\varepsilon}]\|_{L^2(\mathrm{Y}^d)}, \end{aligned} \tag{79}$$

where we used that the Féjer-mean operator gives rise to a bounded linear operator on L^2 with operator norm 1. For the first term, we have, by the estimate (47) for $p = 2$,

$$\|(1 - \phi_N)\boldsymbol{\varepsilon}\|_{L^2(\mathrm{Y}^d)} \leq \|(1 - \phi_N)\|_{L^2(\mathrm{Y}^d)} \|\boldsymbol{\varepsilon}\|_{L^\infty(\mathrm{Y}^d)} \lesssim N^{-\frac{1}{2}}, \tag{80}$$

whereas, for the second term, we observe

$$\begin{aligned} \|\phi_N \boldsymbol{\varepsilon} - F_N[\phi_N \boldsymbol{\varepsilon}]\|_{L^2(\mathrm{Y}^d)} &\lesssim \frac{1}{N} \|\nabla(\phi_N \boldsymbol{\varepsilon})\|_{L^2(\mathrm{Y}^d)} \\ &\lesssim \frac{1}{N} \left(\|(\nabla \phi_N)\boldsymbol{\varepsilon} + \phi_N \nabla \boldsymbol{\varepsilon}\|_{L^2(\mathrm{Y}^d)} \right) \\ &\lesssim \frac{1}{N} \left(\|\nabla \phi_N\|_{L^2(\mathrm{Y}^d)} \|\boldsymbol{\varepsilon}\|_{L^\infty(\mathrm{Y}^d)} + \|\nabla \boldsymbol{\varepsilon}\|_{L^2(\mathrm{Y}^d_\pm)} \right) \\ &\lesssim N^{-\frac{1}{2}}, \end{aligned} \tag{81}$$

where we used the convergence-rate estimate for Féjer approximation (26) and the growth estimate (46) for the gradient of the cut-off function ϕ_N. Thus, the approximation error (77) decays as $N^{-1/2}$.

Let us turn our attention to the interpolation error (78). We would like to apply the error estimate (31) of trigonometric interpolation. However, the integrand is not smooth. As for the approximation error, we use the cut-off function ϕ_N to split the interpolation error (78) into the contributions

$$\begin{aligned}\left\|\mathbb{C} : F_N\boldsymbol{\varepsilon} - Q_N\left[\mathbb{C} : F_N\boldsymbol{\varepsilon}\right]\right\|_{L^2(\mathrm{Y}^d)} &\leq \|(1-\phi_N)\mathbb{C} : F_N\boldsymbol{\varepsilon}\|_{L^2(\mathrm{Y}^d)} \\ &\quad + \left\|\phi_N\mathbb{C} : F_N\boldsymbol{\varepsilon} - Q_N\left[\phi_N\mathbb{C} : F_N\boldsymbol{\varepsilon}\right]\right\|_{L^2(\mathrm{Y}^d)} \\ &\quad + \left\|Q_N\left[(1-\phi_N)\mathbb{C} : F_N\boldsymbol{\varepsilon}\right]\right\|_{L^2(\mathrm{Y}^d)}.\end{aligned} \tag{82}$$

For the first term, we observe

$$\begin{aligned}\|(1-\phi_N)\mathbb{C} : F_N\boldsymbol{\varepsilon}\|_{L^2(\mathrm{Y}^d)} &\leq \|(1-\phi_N)\|_{L^2(\mathrm{Y}^d)}\,\|\mathbb{C} : F_N\boldsymbol{\varepsilon}\|_{L^\infty(\mathrm{Y}^d)} \\ &\leq \overline{\alpha}\,\|(1-\phi_N)\|_{L^2(\mathrm{Y}^d)}\,\|F_N\boldsymbol{\varepsilon}\|_{L^\infty(\mathrm{Y}^d)} \\ &\leq \overline{\alpha}\,\|(1-\phi_N)\|_{L^2(\mathrm{Y}^d)}\,\|\boldsymbol{\varepsilon}\|_{L^\infty(\mathrm{Y}^d)} \\ &\lesssim N^{-\frac{1}{2}},\end{aligned} \tag{83}$$

where we used the decay estimate (47) for $p = 2$ and the crucial property (25) of the Féjer means. Notice that this *would not hold* for the Fourier projection P_N. Using a similar reasoning in view of Parseval's identity (11) permits to bound the third term in the estimate (82)

$$\left\|Q_N\left[(1-\phi_N)\mathbb{C} : F_N\boldsymbol{\varepsilon}\right]\right\|_{L^2(\mathrm{Y}^d)} \lesssim N^{-\frac{1}{2}}. \tag{84}$$

To treat the middle term in the estimate (82), we invoke the error estimate (31) for trigonometric interpolation

$$\left\|\phi_N\mathbb{C} : F_N\boldsymbol{\varepsilon} - Q_N\left[\phi_N\mathbb{C} : F_N\boldsymbol{\varepsilon}\right]\right\|_{L^2(\mathrm{Y}^d)} \lesssim \frac{1}{N^k}\,\left\|\nabla^k\left(\phi_N\mathbb{C} : F_N\boldsymbol{\varepsilon}\right)\right\|_{L^2(\mathrm{Y}^d)}, \quad \text{where} \quad k = \lceil d/2 \rceil. \tag{85}$$

We notice that higher-order derivatives appear on the right-hand side, that is, second derivatives in the physically relevant dimensions $d = 2$ and $d = 3$. However, we may only work with a uniform bound (58) on the strain and the H^1-bounds (59) for the phase strains. To deal with this situation, we utilize the Bernstein estimates (32) and (35). Then, the estimate

$$\left\|\nabla^k\left(\phi_N\mathbb{C} : F_N\boldsymbol{\varepsilon}\right)\right\|_{L^2(\mathrm{Y}^d)} \lesssim N^{k-\frac{1}{2}} \tag{86}$$

can be shown, see Appendix B for details, which in turn implies

$$\left\|\phi_N\mathbb{C} : F_N\boldsymbol{\varepsilon} - Q_N\left[\phi_N\mathbb{C} : F_N\boldsymbol{\varepsilon}\right]\right\|_{L^2(\mathrm{Y}^d)} \lesssim N^{-\frac{1}{2}}. \tag{87}$$

Together with the estimates (83) and (84), we are thus led to the following bound on the interpolation error (82)

$$\left\|\mathbb{C} : F_N\boldsymbol{\varepsilon} - Q_N\left[\mathbb{C} : F_N\boldsymbol{\varepsilon}\right]\right\|_{L^2(\mathrm{Y}^d)} \lesssim N^{-\frac{1}{2}}. \tag{88}$$

In combination with the bound (81) on the approximation error, we are, in view of the decomposition (76), finally led to the estimate (74).

3.4 | Convergence rate for the stress field

The goal of this section is to show the convergence-rate estimate

$$\|\boldsymbol{\sigma} - \boldsymbol{\sigma}_N\|_{L^2(\mathrm{Y}^d)} \lesssim N^{-\frac{1}{2}} \tag{89}$$

for the stress field

$$\boldsymbol{\sigma}_N = Q_N[\mathbb{C} : \boldsymbol{\varepsilon}_N] \in \mathcal{T}_N(\mathrm{Y}^d; \mathrm{Sym}(d)) \tag{90}$$

when approximating the continuous stress field $\boldsymbol{\sigma} = \mathbb{C} : \boldsymbol{\varepsilon}$. Due to the special nature of the Moulinec–Suquet discretization, the convergence estimate (89) does not immediately follow from the established convergence rate (74) for the strain field, as the discretized stress field (90) involves an additional trigonometric interpolation step (13). However, to establish the estimate (89) we may heavily re-use the machinery developed in the previous section. Indeed, recasting the stress error in the form

$$\begin{aligned}\|\boldsymbol{\sigma} - \boldsymbol{\sigma}_N\|_{L^2(\mathrm{Y}^d)} &= \|\mathbb{C} : \boldsymbol{\varepsilon} - Q_N\left[\mathbb{C} : \boldsymbol{\varepsilon}_N\right]\|_{L^2(\mathrm{Y}^d)} \\ &\leq \|\mathbb{C} : (\boldsymbol{\varepsilon} - F_N\boldsymbol{\varepsilon})\|_{L^2(\mathrm{Y}^d)} + \|\mathbb{C} : F_N\boldsymbol{\varepsilon} - Q_N\left[\mathbb{C} : F_N\boldsymbol{\varepsilon}\right]\|_{L^2(\mathrm{Y}^d)} \\ &\quad + \|Q_N\left[\mathbb{C} : (F_N\boldsymbol{\varepsilon} - \boldsymbol{\varepsilon}_N)\right]\|_{L^2(\mathrm{Y}^d)} \\ &\lesssim \|\boldsymbol{\varepsilon} - F_N\boldsymbol{\varepsilon}\|_{L^2(\mathrm{Y}^d)} + \|\mathbb{C} : F_N\boldsymbol{\varepsilon} - Q_N\left[\mathbb{C} : F_N\boldsymbol{\varepsilon}\right]\|_{L^2(\mathrm{Y}^d)} + \|\boldsymbol{\varepsilon} - \boldsymbol{\varepsilon}_N\|_{L^2(\mathrm{Y}^d)},\end{aligned} \tag{91}$$

where we used Parseval's identity (11) and the bound (55) on the stiffness, we recognize the approximation error (77), the interpolation error (78) and the total error (76). For each of these terms, the convergence rate $N^{-1/2}$ was established in the previous section. This shows the validity of the statement (89).

3.5 | Convergence rate for the elastic energy

In this section, we wish to establish a convergence estimate of the form

$$\|\mathbb{C}^{\mathtt{eff}} - \mathbb{C}_N^{\mathtt{eff}}\| \lesssim \frac{1}{N}, \tag{92}$$

that is, the effective stiffness

$$\mathbb{C}_N^{\mathtt{eff}} : \overline{\boldsymbol{\varepsilon}} = \left\langle Q_N\left[\mathbb{C} : \left(\overline{\boldsymbol{\varepsilon}} + \nabla^s \boldsymbol{u}_{\overline{\boldsymbol{\varepsilon}}_N}\right)\right]\right\rangle_Y \tag{93}$$

of the Moulinec–Suquet discretization converges to the continuous effective stiffness (60) with *twice* the rate of the strains (74). In the Galerkin setting, the estimate (92) follows from the estimate for the strain (74) by Galerkin orthogonality, see Ye and Chung[73(Thm. 5)] or Schneider and Wicht[76(§2.2)]. The Moulinec–Suquet discretization[4,5] requires additional arguments to treat the underintegration.

To proceed, we fix a macroscopic strain $\overline{\boldsymbol{\varepsilon}} \in \mathrm{Sym}(d)$ and recall the representation (61)

$$\overline{\boldsymbol{\varepsilon}} : \mathbb{C}^{\mathtt{eff}} : \overline{\boldsymbol{\varepsilon}} = \langle \boldsymbol{\varepsilon} : \mathbb{C} : \boldsymbol{\varepsilon} \rangle_Y, \quad \text{where} \quad \boldsymbol{\varepsilon} = \overline{\boldsymbol{\varepsilon}} + \nabla^s \boldsymbol{u} \tag{94}$$

solves the cell problem (57). For any competition field

$$\tilde{\boldsymbol{\varepsilon}} = \overline{\boldsymbol{\varepsilon}} + \nabla^s \tilde{\boldsymbol{u}} \quad \text{with} \quad \tilde{\boldsymbol{u}} \in H^1_{\#}(\mathrm{Y}^d; \mathbb{R}^d), \tag{95}$$

we expand the square

$$\begin{aligned}\langle (\boldsymbol{\varepsilon} - \tilde{\boldsymbol{\varepsilon}}) : \mathbb{C} : (\boldsymbol{\varepsilon} - \tilde{\boldsymbol{\varepsilon}}) \rangle_Y &= \langle \boldsymbol{\varepsilon} : \mathbb{C} : (\boldsymbol{\varepsilon} - \tilde{\boldsymbol{\varepsilon}}) \rangle_Y - \langle \tilde{\boldsymbol{\varepsilon}} : \mathbb{C} : (\boldsymbol{\varepsilon} - \tilde{\boldsymbol{\varepsilon}}) \rangle_Y \\ &= -\langle \tilde{\boldsymbol{\varepsilon}} : \mathbb{C} : (\boldsymbol{\varepsilon} - \tilde{\boldsymbol{\varepsilon}}) \rangle_Y \\ &= \langle \tilde{\boldsymbol{\varepsilon}} : \mathbb{C} : \tilde{\boldsymbol{\varepsilon}} \rangle_Y - \overline{\boldsymbol{\varepsilon}} : \mathbb{C}^{\mathtt{eff}} : \overline{\boldsymbol{\varepsilon}},\end{aligned} \tag{96}$$

where we used that the difference $\boldsymbol{\varepsilon} - \tilde{\boldsymbol{\varepsilon}} = \nabla^s(\boldsymbol{u} - \tilde{\boldsymbol{u}})$ is a symmetrized gradient and that the field $\boldsymbol{\varepsilon}$ satisfies the equilibrium equation (57). We may rewrite this identity in the form

$$\langle \tilde{\boldsymbol{\varepsilon}} : \mathbb{C} : \tilde{\boldsymbol{\varepsilon}} \rangle_Y = \overline{\boldsymbol{\varepsilon}} : \mathbb{C}^{\mathtt{eff}} : \overline{\boldsymbol{\varepsilon}} + \langle (\boldsymbol{\varepsilon} - \tilde{\boldsymbol{\varepsilon}}) : \mathbb{C} : (\boldsymbol{\varepsilon} - \tilde{\boldsymbol{\varepsilon}}) \rangle_Y. \tag{97}$$

Completely analogous arguments may be applied to the discretized setting for a competition field

$$\tilde{\boldsymbol{\varepsilon}}_N = \overline{\boldsymbol{\varepsilon}} + \nabla^s \tilde{\boldsymbol{u}}_N \quad \text{with} \quad \tilde{\boldsymbol{u}}_N \in \mathcal{T}_N(\mathrm{Y}^d; \mathbb{R}^d), \tag{98}$$

based on the discrete equivalent of Equation (61)

$$\overline{\boldsymbol{\varepsilon}} : \mathbb{C}_N^{\mathtt{eff}} : \overline{\boldsymbol{\varepsilon}} = \left\langle \boldsymbol{\varepsilon}_N : Q_N \left[\mathbb{C} : \boldsymbol{\varepsilon}_N \right] \right\rangle_Y , \tag{99}$$

to yield

$$\left\langle \tilde{\boldsymbol{\varepsilon}}_N : Q_N \left[\mathbb{C} : \tilde{\boldsymbol{\varepsilon}}_N \right] \right\rangle_Y = \overline{\boldsymbol{\varepsilon}} : \mathbb{C}_N^{\mathtt{eff}} : \overline{\boldsymbol{\varepsilon}} + \left\langle (\boldsymbol{\varepsilon}_N - \tilde{\boldsymbol{\varepsilon}}_N) : Q_N \left[\mathbb{C} : (\boldsymbol{\varepsilon}_N - \tilde{\boldsymbol{\varepsilon}}_N) \right] \right\rangle_Y . \tag{100}$$

Subtracting the identity (97) with $\tilde{\boldsymbol{\varepsilon}} = \tilde{\boldsymbol{\varepsilon}}_N$ from the previous line (100) provides the exact expression

$$\begin{aligned} \overline{\boldsymbol{\varepsilon}} : \left(\mathbb{C}^{\mathtt{eff}} - \mathbb{C}_N^{\mathtt{eff}} \right) : \overline{\boldsymbol{\varepsilon}} = & \langle \tilde{\boldsymbol{\varepsilon}}_N : \mathbb{C} : \tilde{\boldsymbol{\varepsilon}}_N \rangle_Y - \left\langle \tilde{\boldsymbol{\varepsilon}}_N : Q_N \left[\mathbb{C} : \tilde{\boldsymbol{\varepsilon}}_N \right] \right\rangle_Y \\ & + \left\langle (\boldsymbol{\varepsilon}_N - \tilde{\boldsymbol{\varepsilon}}_N) : Q_N \left[\mathbb{C} : (\boldsymbol{\varepsilon}_N - \tilde{\boldsymbol{\varepsilon}}_N) \right] \right\rangle_Y - \langle (\boldsymbol{\varepsilon} - \tilde{\boldsymbol{\varepsilon}}_N) : \mathbb{C} : (\boldsymbol{\varepsilon} - \tilde{\boldsymbol{\varepsilon}}_N) \rangle_Y . \end{aligned} \tag{101}$$

Taking norms thus leads us to the estimate

$$\begin{aligned} \left\| \overline{\boldsymbol{\varepsilon}} : \left(\mathbb{C}^{\mathtt{eff}} - \mathbb{C}_N^{\mathtt{eff}} \right) : \overline{\boldsymbol{\varepsilon}} \right\| \lesssim & \left| \langle \tilde{\boldsymbol{\varepsilon}}_N : \mathbb{C} : \tilde{\boldsymbol{\varepsilon}}_N \rangle_Y - \left\langle \tilde{\boldsymbol{\varepsilon}}_N : Q_N \left[\mathbb{C} : \tilde{\boldsymbol{\varepsilon}}_N \right] \right\rangle_Y \right| \\ & + \| \boldsymbol{\varepsilon}_N - \tilde{\boldsymbol{\varepsilon}}_N \|^2_{L^2(\mathrm{Y}^d)} + \| \boldsymbol{\varepsilon} - \tilde{\boldsymbol{\varepsilon}}_N \|^2_{L^2(\mathrm{Y}^d)}, \end{aligned} \tag{102}$$

where we used Parseval's identity (11) and the upper bound (55) on the stiffness. Taking Féjer means

$$\tilde{\boldsymbol{\varepsilon}}_N = F_N \boldsymbol{\varepsilon}, \tag{103}$$

the results of the previous section, that is, the estimate (74), permit us to conclude that the estimate

$$\| \boldsymbol{\varepsilon}_N - \tilde{\boldsymbol{\varepsilon}}_N \|^2_{L^2(\mathrm{Y}^d)} + \| \boldsymbol{\varepsilon} - \tilde{\boldsymbol{\varepsilon}}_N \|^2_{L^2(\mathrm{Y}^d)} \lesssim \frac{1}{N} \tag{104}$$

holds. Therefore, in view of the goal (92), it is necessary to study the *quadrature error*

$$\langle \tilde{\boldsymbol{\varepsilon}}_N : \mathbb{C} : \tilde{\boldsymbol{\varepsilon}}_N \rangle_Y - \left\langle \tilde{\boldsymbol{\varepsilon}}_N : Q_N \left[\mathbb{C} : \tilde{\boldsymbol{\varepsilon}}_N \right] \right\rangle_Y = \langle \tilde{\boldsymbol{\varepsilon}}_N : \mathbb{C} : \tilde{\boldsymbol{\varepsilon}}_N \rangle_Y - \frac{1}{N^d} \sum_{x_I \in \mathrm{Y}_N^d} \tilde{\boldsymbol{\varepsilon}}_N(x_I) : \mathbb{C}(x_I) : \tilde{\boldsymbol{\varepsilon}}_N(x_I) \tag{105}$$

in the estimate (102), where we used the fact (take Equation (11) with $g_N \equiv 1$) that trigonometric polynomials of degree N are integrated *exactly* by the trapezoidal rule of order N.

To proceed, let us introduce the field

$$\tilde{\mathbb{E}}_N = \tilde{\boldsymbol{\varepsilon}}_N \otimes \tilde{\boldsymbol{\varepsilon}}_N \in \mathcal{T}_{2N}(\mathrm{Y}^d; \mathrm{Sym}(d) \otimes \mathrm{Sym}(d)), \tag{106}$$

which is a trigonometric polynomial of order $2N$ with values in fourth-order tensors, and rewrite the quadrature error (105) in the slightly shorter form

$$\langle \tilde{\boldsymbol{\varepsilon}}_N : \mathbb{C} : \tilde{\boldsymbol{\varepsilon}}_N \rangle_Y - \frac{1}{N^d} \sum_{x_I \in \mathrm{Y}_N^d} \tilde{\boldsymbol{\varepsilon}}_N(x_I) : \mathbb{C}(x_I) : \tilde{\boldsymbol{\varepsilon}}_N(x_I) = \left\langle \mathbb{C} :: \tilde{\mathbb{E}}_N \right\rangle_Y - \frac{1}{N^d} \sum_{x_I \in \mathrm{Y}_N^d} \mathbb{C}(x_I) :: \tilde{\mathbb{E}}_N(x_I). \tag{107}$$

We wish to apply the quadrature estimate (50). However, the integrand $\mathbb{C} :: \tilde{\mathbb{E}}_N$ is discontinuous due to the discontinuous stiffness $\mathbb{C}$. Therefore, we invoke the splitting

$$\begin{aligned} \left\langle \mathbb{C} :: \tilde{\mathbb{E}}_N \right\rangle_Y - \frac{1}{N^d} \sum_{x_I \in \mathrm{Y}_N^d} \mathbb{C}(x_I) :: \tilde{\mathbb{E}}_N(x_I) = & \left\langle (1 - \phi_N) \mathbb{C} :: \tilde{\mathbb{E}}_N \right\rangle_Y \\ & + \left\langle \phi_N \mathbb{C} :: \tilde{\mathbb{E}}_N \right\rangle_Y - \frac{1}{N^d} \sum_{x_I \in \mathrm{Y}_N^d} \phi_N(x_I) \mathbb{C}(x_I) :: \tilde{\mathbb{E}}_N(x_I) \\ & + \frac{1}{N^d} \sum_{x_I \in \mathrm{Y}_N^d} (1 - \phi_N(x_I)) \mathbb{C}(x_I) :: \tilde{\mathbb{E}}_N(x_I) \end{aligned} \tag{108}$$

in terms of the cut-off function ϕ_N, introduced in Equation (40). For the first term, we observe

$$\left\langle (1-\phi_N)\mathbb{C} :: \tilde{\mathbb{E}}_N \right\rangle_Y \leq \alpha_+ \|1-\phi_N\|_{L^1(\mathrm{Y}^d)} \|\boldsymbol{\varepsilon}\|^2_{L^\infty(\mathrm{Y}^d)} \lesssim \frac{1}{N}, \tag{109}$$

where we used Hölder's inequality, the bound on the stiffness (55), the definition (106) of the field $\tilde{\mathbb{E}}_N$, the property (25) of Féjer means and the inequality (47) for $p = 1$. With a completely analogous argument, the estimate

$$\frac{1}{N^d} \sum_{x_I \in \mathrm{Y}^d_N} (1-\phi_N(x_I))\mathbb{C}(x_I) :: \tilde{\mathbb{E}}_N(x_I) \lesssim \frac{1}{N}, \tag{110}$$

is readily seen to hold. To treat the quadrature error in the middle of the right hand side of equation (108), we make use of the quadrature estimate (50)

$$\left| \left\langle \phi_N \mathbb{C} :: \tilde{\mathbb{E}}_N \right\rangle_Y - \frac{1}{N^d} \sum_{x_I \in \mathrm{Y}^d_N} \phi_N(x_I)\mathbb{C}(x_I) :: \tilde{\mathbb{E}}_N(x_I) \right| \lesssim \sum_{\|\alpha\|_\infty = 1} \frac{1}{N^{|\alpha|}} \left\| \partial^\alpha \left(\phi_N \mathbb{C} :: \tilde{\mathbb{E}}_N \right) \right\|_{L^1(\mathrm{Y}^d)}. \tag{111}$$

To get an idea how to handle the terms on the right-hand side, we compute the first ($j = 1, 2, \dots, d$)

$$\partial_j \left(\phi_N \mathbb{C} :: \tilde{\mathbb{E}}_N \right) = \partial_j \phi_N \mathbb{C} :: \tilde{\mathbb{E}}_N + 2\phi_N \mathbb{C} :: \tilde{\boldsymbol{\varepsilon}}_N \otimes \partial_j \tilde{\boldsymbol{\varepsilon}}_N \tag{112}$$

and the second derivative ($j, k = 1, 2, \dots, d$)

$$\begin{aligned} \partial_k \partial_j \left(\phi_N \mathbb{C} :: \tilde{\mathbb{E}}_N \right) = {} & \partial_k \partial_j \phi_N \mathbb{C} :: \tilde{\mathbb{E}}_N \\ & + 2\partial_j \phi_N \mathbb{C} :: \tilde{\boldsymbol{\varepsilon}}_N \otimes \partial_k \tilde{\boldsymbol{\varepsilon}}_N \\ & + 2\partial_k \phi_N \mathbb{C} :: \tilde{\boldsymbol{\varepsilon}}_N \otimes \partial_j \tilde{\boldsymbol{\varepsilon}}_N \\ & + 2\phi_N \mathbb{C} :: \partial_k \tilde{\boldsymbol{\varepsilon}}_N \otimes \partial_j \tilde{\boldsymbol{\varepsilon}}_N \\ & + 2\phi_N \mathbb{C} :: \tilde{\boldsymbol{\varepsilon}}_N \otimes \partial_k \partial_j \tilde{\boldsymbol{\varepsilon}}_N \end{aligned} \tag{113}$$

explicitly. From the expression (112), we estimate

$$\left\| \partial_j \left(\phi_N \mathbb{C} :: \tilde{\mathbb{E}}_N \right) \right\|_{L^2(\mathrm{Y}^d)} \lesssim \|\nabla \phi_N\|_{L^1(\mathrm{Y}^d)} \|\boldsymbol{\varepsilon}\|^2_{L^\infty(\mathrm{Y}^d)} + \|\boldsymbol{\varepsilon}\|_{L^\infty(\mathrm{Y}^d)} \|\boldsymbol{\varepsilon}\|_{H^1(\mathrm{Y}^d_\pm)} \lesssim 1, \tag{114}$$

where the critical ingredient is the L^1-bound (46). The first term on the right hand side of Equation (113) may be handled as follows

$$\left\| \partial_k \partial_j \phi_N \mathbb{C} :: \tilde{\mathbb{E}}_N \right\|_{L^1(\mathrm{Y}^d)} \lesssim N \ \|\boldsymbol{\varepsilon}\|^2_{L^\infty} \tag{115}$$

by the estimate (45) for $p = 1$ and $|\alpha| = 2$. To treat the second term in the identity (113), we notice

$$\begin{aligned} \left\| \partial_j \phi_N \mathbb{C} :: \tilde{\boldsymbol{\varepsilon}}_N \otimes \partial_k \tilde{\boldsymbol{\varepsilon}}_N \right\|_{L^1(\mathrm{Y}^d)} &\lesssim \left\| \partial_j \phi_N \right\|_{L^1(\mathrm{Y}^d)} \|\boldsymbol{\varepsilon}\|_{L^\infty(\mathrm{Y}^d)} \|\partial_k \tilde{\boldsymbol{\varepsilon}}_N\|_{L^\infty(\mathrm{Y}^d)} \\ &\lesssim N \ \|\boldsymbol{\varepsilon}\|_{L^\infty(\mathrm{Y}^d)} \|\tilde{\boldsymbol{\varepsilon}}_N\|_{L^\infty(\mathrm{Y}^d)} \\ &\lesssim N \ \|\boldsymbol{\varepsilon}\|^2_{L^\infty(\mathrm{Y}^d)}, \end{aligned} \tag{116}$$

where, apart from the uniform L^1-bound (46) the Bernstein estimate (32) is crucial to remove the derivative from the L^∞-estimate for the trigonometric polynomial $\tilde{\boldsymbol{\varepsilon}}_N$. The other terms in Equation (113) can be estimated with similar ideas to obtain the bound

$$\left\| \partial_k \partial_j \left(\phi_N \mathbb{C} :: \tilde{\mathbb{E}}_N \right) \right\|_{L^1(\mathrm{Y}^d)} \lesssim N. \tag{117}$$

Actually, completely analogous arguments may be used to derive the estimate

$$\left\| \partial^\alpha \left(\phi_N \mathbb{C} :: \tilde{\mathbb{E}}_N \right) \right\|_{L^1(\mathrm{Y}^d)} \lesssim N^{|\alpha|-1} \tag{118}$$

for higher derivatives, as well. Thus, in view of the bound (111), we are led to the estimate

$$\left| \left\langle \phi_N \mathbb{C} :: \tilde{\mathbb{E}}_N \right\rangle_Y - \frac{1}{N^d} \sum_{x_I \in \mathrm{Y}_N^d} \phi_N(x_I) \mathbb{C}(x_I) :: \tilde{\mathbb{E}}_N(x_I) \right| \lesssim \frac{1}{N}. \tag{119}$$

Together with the estimates (109) and (110), the bound

$$\left| \langle \tilde{\boldsymbol{\varepsilon}}_N : \mathbb{C} : \tilde{\boldsymbol{\varepsilon}}_N \rangle_Y - \left\langle \tilde{\boldsymbol{\varepsilon}}_N : Q_N \left[\mathbb{C} : \tilde{\boldsymbol{\varepsilon}}_N \right] \right\rangle_Y \right| \lesssim \frac{1}{N} \tag{120}$$

on the quadrature error (105) emerges. Combined with the quadratic estimates (104), the derivation of the desired statement (92) is complete.

4 | COMPUTATIONAL INVESTIGATIONS

The goal of this section is to provide computational results showing that the obtained convergence rates for the local strain and stress fields as well as for the effective stiffness are actually attained upon grid refinement. Indeed, our considerations could be suboptimal, requiring more elaborate mathematical techniques to derive optimal rates.

We relied upon an in-house FFT-based computational homogenization code,[41] run on a workstation with two AMD EPYC 7642 with 48 physical cores each. To handle discretizations with an *even* number of voxels in certain coordinate directions, the values of the *strain field* are set to zero at the Nyquist frequencies. For every considered mesh size, the equilibrium equation (64) was solved to an accuracy of 10^{-5} w.r.t. the "natural" convergence criterion[14(§3.6)]. Then, the effective stresses were computed by volume averaging.

We consider a microstructure with a single spherical inclusion placed at the center of the microstructure, see Figure 1A, with a volume fraction of 6.54%. The isotropic linear elastic material parameters are listed in Table 1, corresponding to a polyamide matrix and an E-glass filler. The considered microstructure satisfies the conditions presented in Section 2.2, in particular the smoothness of the interface, required for the Li-Nirenberg estimates to hold, see Section 3.1. Thus, the theory developed in this article applies. We load the structure via a shear in the x-y-plane.

The highest considered resolution, 512^3 voxels, is taken as the reference. Then, the relative errors of the strain and stress field, both measured in $L^2(\mathrm{Y}^d)$, and the effective stress are shown in Figure 1B. We observe that the local solution fields, that is, the strain and the stress fields, show an $N^{-1/2}$ convergence rate, as predicted by the theory, see estimates

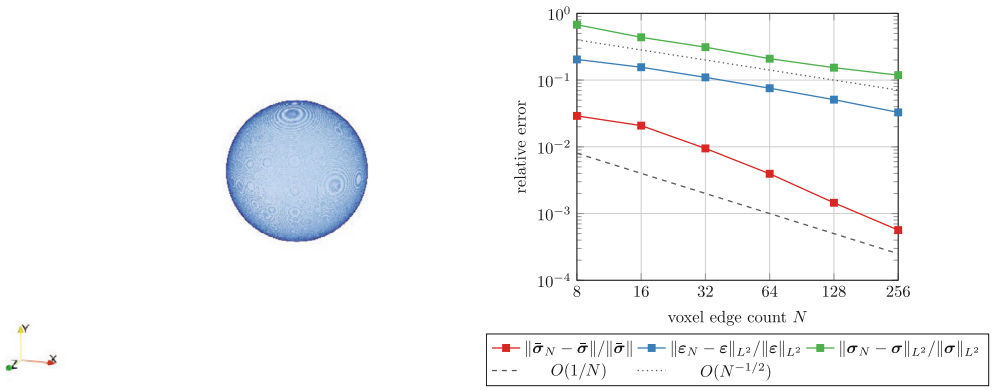

FIGURE 1 The single spherical inclusion. (A) Microstructure, (B) Convergence rates.

TABLE 1 Material parameters considered for the computational experiments.[100]

Inclusion(s)	$E = 72$ GPa	$\nu = 0.22$
Matrix	$E = 2.1$ GPa	$\nu = 0.3$

(74) and (89). The effective stress, on the other hand, converges much faster, and shows roughly an N^{-1}-rate, as predicted by our derivations, see the estimate (92).

The previous example was admittedly simple in order to enable going to fine resolutions and satisfying all the requirements of the theory.

We retain the material models and parameters of the previous example, but investigate a more complex short-fiber reinforced microstructure. More precisely, we take a look at a material reinforced by 20% E-glass fibers with an aspect ratio of ten and a second-order fiber-orientation tensor[101,102]

$$A = \mathtt{diag}(0.45, 0.45, 0.1), \tag{121}$$

which describes a small deviation from a planar isotropic fiber-orientation state. As the fibers are described by cylinders, the interface between matrix and inclusions does not satisfy the $C^{1,\alpha}$-condition required for the Li–Nirenberg estimates,[91] and the theory developed in this article does not apply.

The microstructure has dimensions $256 \times 256 \times 64$ μm^3, shown in Figure 2A and contains 106 fibers. It was generated by the SAM[103] algorithm, employing the exact closure approximation.[104]

We consider resolutions $N \times N \times N/4$ with discretization parameters N in the set $\{64, 128, 256, \dots, 1024\}$. A non-cubical microstructure is used to permit considering a larger resolution in the principal fiber directions. Indeed, due to the anisotropic reinforcements, higher stresses are expected in-plane compared to out-of-plane. We apply a shear strain in the 1-2-plane, that is, in the fiber plane. The computation with $N = 1024$ serves as our reference.

The relative errors of the stress and the strain field (in L^2) as well as the convergence of the effective stress is shown in Figure 2B. We observe that the local fields converge as $N^{-1/2}$ in the L^2-norm. Moreover, the errors in the effective stresses decay as $1/N$. In particular, the convergence asymptotics match the simpler spherical case which we considered previously.

We conclude this section by investigating a microstructure where an analytic solution for the local solution fields is available, at least for a specific macroscopic loading. More precisely, we consider the neutral inclusion introduced by Hashin.[105]

The microstructure consists of three phases, a spherical core

$$\Omega_1 = \left\{ x \in \mathrm{Y}^d \;\middle|\; \|x - x_c\| < r_1 \right\}, \tag{122}$$

an annular region

$$\Omega_2 = \left\{ x \in \mathrm{Y}^d \;\middle|\; r_1 < \|x - x_c\| < r_2 \right\} \tag{123}$$

and the remaining "matrix"

$$\Omega_3 = \left\{ x \in \mathrm{Y}^d \;\middle|\; \|x - x_c\| > r_2 \right\} \tag{124}$$

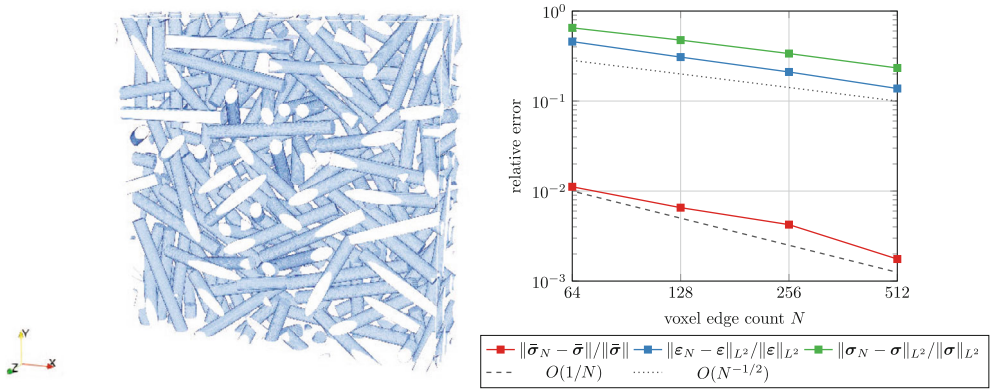

(A) (B)

FIGURE 2 The almost planar fiber-reinforced composite. (A) Microstructure, (B) Convergence rates.

with the geometric center $x_c = (\pi, \pi, \pi)$ of the microstructure and two radii $r_1 < r_2 < 2\pi$. Each of these three phases is occupied by an isotropic elastic medium. Hashin[105] showed that under macroscopic compression it is possible to select the elastic moduli of the phases Ω_1 and Ω_2 in such a way that the effective compression modulus of the microstructure coincides with the compression modulus of the matrix phase. The shear moduli μ_1 and μ_3 of the core and the matrix are actually irrelevant for the consideration. Typically, we fix the compression modulus $K_3 \equiv K^{\mathtt{eff}}$ of the matrix and the ratio K_2/μ_2 of the intermediate region. There is a relationship[105] between the compression moduli K_1 and K_2, that is,

$$K_1 = K_2 + \frac{K^{\mathtt{eff}} - K_2}{\phi_1 - \phi_2 \frac{K^{\mathtt{eff}} - K_2}{K_2 + \frac{4}{3}\mu_2}}, \tag{125}$$

where $\phi_1 = (r_1/r_2)^3$ and $\phi_2 = 1 - \phi_1$. For our investigation at hand, there are two cases to consider. For the first case, which we term "porous", the compression modulus K_1 is less than $K_3 \equiv K^{\mathtt{eff}}$. It follows that the compression modulus K_2 of the intermediate region exceeds $K_3 \equiv K^{\mathtt{eff}}$. With decreasing K_1, K_2 increases. However, as K_1 goes the zero, K_2 remains bounded. Thus, we approach the case of a single pore with a special coating embedded in the matrix.

In the second case, which we call "rigid", the compression modulus K_1 exceeds $K_3 \equiv K^{\mathtt{eff}}$, whereas K_2 is smaller than $K_3 \equiv K^{\mathtt{eff}}$. For increasing K_1, K_2 decreases. As $K_1 \to \infty$, K_2 remains bounded away from zero. Thus, in the limit $K_1 \to \infty$, we are faced with a rigid inclusion with special coating inside the matrix.

These two scenarios permit us to consider different material contrasts

$$\kappa = \frac{\max_{i=1,2,3} K_i}{\min_{i=1,2,3} K_i} \tag{126}$$

in the compression modulus.

For the study at hand, We use the radii

$$r_1 = \frac{200}{1024}\,\pi e \quad \text{and} \quad r_2 = \frac{300}{1024}\,\pi^2, \tag{127}$$

where $e = \sum_{k=0}^{\infty} \frac{1}{k!}$ is Euler's number. We set $K^{\mathtt{eff}} = 1/3$ and fix $\mu_i = K_i$ $(i = 1, 2, 4)$, that is, we set Poisson's ratio to $\nu_i = 1/8$ $(i = 1, 2, 3)$. We compare the relative error in the effective compression modulus and the L^2-error of the local strain and stress fields, see Figure 3. Inspecting the error in the effective properties for the "porous" case, see Figure 3A, we observe that the two coarsest discretizations, $N = 16$ and $N = 32$, do not conform to the expected scaling $1/N$. This contrasts with the geometries previously considered in this section, and is caused by the comparatively coarse resolution of the regions Ω_1 and Ω_2. For the finer discretizations the theoretically predicted $1/N$-convergence rate is confirmed. We observe that the error increases with the contrast, with no clear limit as $\kappa \to \infty$.

For the "rigid" case, see Figure 3B, the behavior is similar, and more or less the same conclusions may be drawn. However, the errors are slightly larger than for the "porous" case. Please note that resolving the latter is computationally much more expensive than dealing with the "porous" case due to the primal formulation. A remedy consists in working with the dual formulation.[62,106]

Taking a look at the local L^2-strain error of the "porous" case, see Figure 3C, we also observe no clear trend in the convergence behavior for low resolution due to the geometric error induced by the coarse voxelation. Only for the highest resolutions, the theoretically predicted $N^{-1/2}$ convergence behavior is clearly seen. We observe that the strain error increases with the contrast, even strongly so. Keeping in mind that the axes are scaled logarithmically, a divergence of the strain error is evident. This behavior is a well-known and understood characteristic of the Moulinec–Suquet discretization.[47,50,57]

Taking a look at the stress error for the "porous" case, see Figure 3E, we observe a completely different behavior. As the contrast κ increases to infinity, there is a clear saturation behavior of the stress error, following the predicted $N^{-1/2}$-rate.

For the "rigid" case, see Figure 3E,F, the roles of stress and strain are reversed—as expected—but the conclusions to be drawn remain the same.

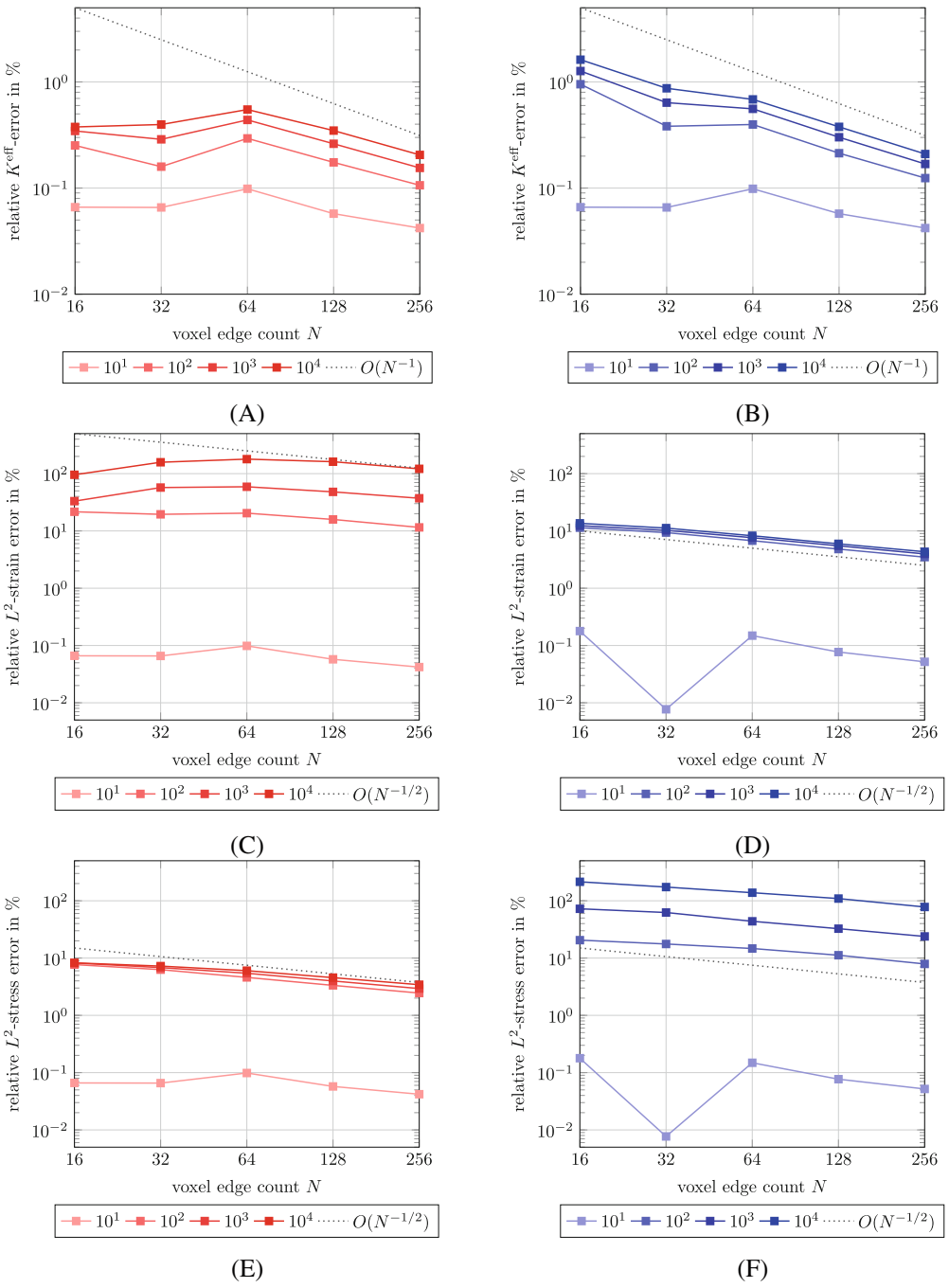

FIGURE 3 Convergence behavior of the effective compression modulus as well as the local strain and stress fields for Hashin's sphere for different contrasts κ, see Equation (126). The "porous" case is shown on the left, and the "rigid" case on the right. (A) $|K_N^{\text{eff}} - K^{\text{eff}}|/K^{\text{eff}}, K_1 < K^{\text{eff}}$, (B) $|K_N^{\text{eff}} - K^{\text{eff}}|/K^{\text{eff}}, K_1 > K^{\text{eff}}$, (C) $\|\varepsilon_N - \varepsilon\|_{L^2}/\|\varepsilon\|_{L^2}, K_1 < K^{\text{eff}}$, (D) $\|\varepsilon_N - \varepsilon\|_{L^2}/\|\varepsilon\|_{L^2}, K_1 > K^{\text{eff}}$, (E) $\|\sigma_N - \sigma\|_{L^2}/\|\sigma\|_{L^2}, K_1 < K^{\text{eff}}$, (D) $\|\sigma_N - \sigma\|_{L^2}/\|\sigma\|_{L^2}, K_1 > K^{\text{eff}}$.

5 | CONCLUSION

The goal of this article was to provide a sharp error analysis for the Moulinec–Suquet discretization,[4,5] providing the theoretical basis for its practical success in computational micromechanics. Previous works were mostly restricted to qualitative convergence results.[66,72,73] The only quantitative results that we are aware of either require higher smoothness of the coefficients,[71] are restricted to specific microstructures, that is, laminates,[107] or deal with the Galerkin setup.[108]

The principal difficulty involved was the low regularity characterizing the solution of the micromechanical problem and composite materials. Indeed, both the stress and the strain fields are, in general, discontinuous across material interfaces, a situation that is inherently linked to the physics of the problem.

We employed a strategy based on smoothing and elementary energy estimates to deal with the problem, losing half of the optimal $1/N$-rate in the process due to balancing the smoothing and the approximation error. Moreover, we could handle the higher derivatives appearing in the interpolation estimates by using Bernstein estimates for the gradient of the trigonometric polynomial. Usually it is better to work out estimates in terms of the non-discretized, that is, continuous, solution field. In our case, the opposite strategy turned out to be vital. Another key ingredient of the approach is the use of Féjer means to be able to preserve the L^∞-bound upon trigonometric approximation. It would be interesting to see whether this theoretical tool is also useful for practical matters.

In addition to providing rates for the strain and the stress fields in L^2, we also investigated the error of the effective stiffness (or the effective stresses). For this purpose, we took a close look at the error induced by trigonometric interpolation. On top of the Ye–Chung superconvergence argument,[73] a similar reasoning as for the strain/stress estimates was necessary, replacing the L^2- by L^1-estimates.

Let us take a critical look at the assumptions and possibilities for future work. This work was restricted to linear elasticity and smooth material interfaces as we relied critically on the Li–Nirenberg estimates[91] which were formulated in this setting. Suitable a-priori estimates[72] and a Ye–Chung type argument[76] are available for more general stress operators of strongly monotone type. Thus, generalizations of the Li–Nirenberg estimates to this kind of nonlinearity would probably enable extending the work at hand to this more general case, as well. Actually, computational experiments[76] suggest that the reported rates also hold for relevant classes of nonlinear composites and interesting classes of non-smooth material interfaces. To treat the latter analytically, finer tools are required, for example, based on weighted function spaces.[109,110]

Another intriguing question concerns whether it is possible to design computational methods on Cartesian grids which converge at a higher rate than the Moulinec–Suquet discretization (and its relatives), but comes with a similar computational efficiency, for example, by using the fast Fourier transform.

ACKNOWLEDGMENTS

Support by the Deutsche Forschungsgemeinschaft (DFG, German Research Foundation)–255730231–and the European Research Council within the Horizon Europe program–project 101040238–is gratefully acknowledged. The author is grateful to D. Knees for shedding light on some results of regularity theory of elliptic systems, L. Risthaus for constructive feedback on an initial version of the manuscript and the anonymous reviewers for carefully reading the submitted manuscript. Open Access funding enabled and organized by Projekt DEAL.

DATA AVAILABILITY STATEMENT

The data that support the findings of this study are available from the corresponding author upon reasonable request.

ORCID

Matti Schneider https://orcid.org/0000-0001-7017-3618

REFERENCES

1. Matouš K, Geers MGD, Kouznetsova VG, Gillman A. A review of predictive nonlinear theories for multiscale modeling of heterogeneous materials. *J Comput Phys*. 2017;330:192-220.
2. Landis EN, Keane DT. X-ray microtomography. *Mater Charact*. 2010;61:1305-1316.
3. Guven I, Cinar K. Micromechanical modeling of particulate-filled composites using micro-CT to create representative volume elements. *Int J Mech Mater Des*. 2019;15:695-714.
4. Moulinec H, Suquet P. A fast numerical method for computing the linear and nonlinear mechanical properties of composites. *Comptes Rendus Acad Sci II*. 1994;318(11):1417-1423.
5. Moulinec H, Suquet P. A numerical method for computing the overall response of nonlinear composites with complex microstructure. *Comput Methods Appl Mech Eng*. 1998;157:69-94.
6. Lahellec N, Michel JC, Moulinec H, Suquet P. Analysis of inhomogeneous materials at large strains using fast Fourier transforms. In: Miehe C, ed. *IUTAM Symposium on Computational mechanics of Solid Materials at Large Strains*. Solid Mechanics and Its Applications. Vol 108. Springer; 2003:247-258.
7. Kabel M, Böhlke T, Schneider M. Efficient fixed point and Newton-Krylov solvers for FFT-based homogenization of elasticity at large deformations. *Comput Mech*. 2014;54(6):1497-1514.
8. de Geus TW, Vondřejc J, Zeman J, Peerlings RHJ, Geers MGD. Finite strain FFT-based non-linear solvers made simple. *Comput Methods Appl Mech Eng*. 2017;318:412-430.

9. Brenner R. Computational approach for composite materials with coupled constitutive laws. *Z Angew Math Phys*. 2010;61(919–927):1-15.
10. Rambausek M, Göküzüm FS, Nguyen LTK, Keip M-A. A two-scale FE-FFT approach to nonlinear magneto-elasticity. *Int J Numer Methods Eng*. 2019;117:1117-1142.
11. Wicht D, Schneider M, Böhlke T. Computing the effective response of heterogeneous materials with thermomechanically coupled constituents by an implicit FFT-based approach. *Int J Numer Methods Eng*. 2021;122(5):1307-1332.
12. Segurado J, Lebensohn RA, Lorca JL. Chapter one—Computational homogenization of polycrystals. *Adv Appl Mech*. 2018;51:1-114.
13. Lebensohn RA, Rollett AD. Spectral methods for full-field micromechanical modelling of polycrystalline material. *Comput Mater Sci*. 2020;173:109336.
14. Schneider M. A review of non-linear FFT-based computational homogenization methods. *Acta Mech*. 2021;232:2051-2100.
15. Beran MJ. *Statistical Contimuum Theories*. Wiley; 1968.
16. Willis JR. Variational and related methods for the overall properties of composites. *Adv Appl Mech*. 1981;21:1-78.
17. Milton GW. *The Theory of Composites*. Cambridge University Press; 2002.
18. Torquato S. *Random Heterogeneous Materials – Microstructure and Macroscopic Properties*. Springer; 2002.
19. Zeller R, Dederichs PH. Elastic constants of polycrystals. *Phys Status Solidi*. 1973;55(2):831-842.
20. Kröner E. Bounds for effective elastic moduli of disordered materials. *J Mech Phys Solids*. 1977;25(2):137-155.
21. Mura T. *Micromechanics of Defects in Solids*. Martinus Nijhoff; 1987.
22. Brisard S, Dormieux L. FFT-based methods for the mechanics of composites: a general variational framework. *Comput Mater Sci*. 2010;49(3):663-671.
23. Ernesti F, Schneider M, Böhlke T. Fast implicit solvers for phase field fracture problems on heterogeneous microstructures. *Comput Methods Appl Mech Eng*. 2020;363:112793.
24. Eyre DJ, Milton GW. A fast numerical scheme for computing the response of composites using grid refinement. *Eur Phys J Appl Phys*. 1999;6(1):41-47.
25. Sen AK, Torquato S. Effective conductivity of anisotropic two-phase composite media. *Phys Rev B*. 1989;39:4504-4515.
26. Torquato S. Effective stiffness tensor of composite media. I. Exact series expansions. *J Mech Phys Solids*. 1997;45:1421-1448.
27. Michel JC, Moulinec H, Suquet P. A computational method based on augmented Lagrangians and fast Fourier transforms for composites with high contrast. *Comput Model Eng Sci*. 2000;1(2):79-88.
28. Michel JC, Moulinec H, Suquet P. A computational scheme for linear and non-linear composites with arbitrary phase contrast. *Int J Numer Methods Eng*. 2001;52:139-160.
29. Monchiet V, Bonnet G. A polarization-based FFT iterative scheme for computing the effective properties of elastic composites with arbitrary contrast. *Int J Numer Methods Eng*. 2012;89:1419-1436.
30. Monchiet V, Bonnet G. Numerical homogenization of nonlinear composites with a polarization-based FFT iterative scheme. *Comput Mater Sci*. 2013;79:276-283.
31. Eisenlohr P, Diehl M, Lebensohn RA, Roters F. A spectral method solution to crystal elasto-viscoplasticity at finite strains. *Int J Plast*. 2013;46:37-53.
32. Schneider M. An FFT-based method for computing weighted minimal surfaces in microstructures with applications to the computational homogenization of brittle fracture. *Int J Numer Methods Eng*. 2020;121:1367-1387.
33. Willot F. The effective conductivity of strongly nonlinear media: the dilute limit. *Int J Solids Struct*. 2020;184:287-295.
34. Ernesti F, Schneider M. A fast fourier transform based method for computing the effective crack energy of a heterogeneous material on a combinatorially consistent grid. *Int J Numer Methods Eng*. 2021;122:6283-6307.
35. Schneider M, Wicht D, Böhlke T. On polarization-based schemes for the FFT-based computational homogenization of inelastic materials. *Comput Mech*. 2019;64(4):1073-1095.
36. Schneider M. On non-stationary polarization methods in FFT-based computational micromechanics. *Int J Numer Methods Eng*. 2021;122(22):6800-6821.
37. Gélébart L, Mondon-Cancel R. Non-linear extension of FFT-based methods accelerated by conjugate gradients to evaluate the mechanical behavior of composite materials. *Comput Mater Sci*. 2013;77:430-439.
38. Zeman J, Vondřejc J, Novák J, Marek I. Accelerating a FFT-based solver for numerical homogenization of periodic media by conjugate gradients. *J Comput Phys*. 2010;229(21):8065-8071.
39. Schneider M. A dynamical view of nonlinear conjugate gradient methods with applications to FFT-based computational micromechanics. *Comput Mech*. 2020;66:239-257.
40. Chen Y, Gélébart L, Chateau C, Bornert M, Sauder C, King A. Analysis of the damage initiation in a SiC/SiC composite tube from a direct comparison between large-scale numerical simulation and synchrotron X-ray micro-computed tomography. *Int J Solids Struct*. 2019;161:111-126.
41. Schneider M. On the Barzilai-Borwein basic scheme in FFT-based computational homogenization. *Int J Numer Methods Eng*. 2019;118(8):482-494.
42. Wicht D, Schneider M, Böhlke T. On Quasi-Newton methods in FFT-based micromechanics. *Int J Numer Methods Eng*. 2020;121(8):1665-1694.
43. Gibbs JW. Fourier's series. *Nature*. 1898;59(1522):200.
44. Müller WH. Mathematical vs. experimental stress analysis of inhomogeneities in solids. *J Phys IV*. 1996;6:C1.139-C1.148.
45. Willot F, Abdallah B, Pellegrini Y-P. Fourier-based schemes with modified Green operator for computing the electrical response of heterogeneous media with accurate local fields. *Int J Numer Methods Eng*. 2014;98:518-533.

46. Willot F. Fourier-based schemes for computing the mechanical response of composites with accurate local fields. *Comptes Rendus Mécanique*. 2015;343:232-245.
47. Schneider M, Merkert D, Kabel M. FFT-based homogenization for microstructures discretized by linear hexahedral elements. *Int J Numer Methods Eng*. 2017;109:1461-1489.
48. Leuschner M, Fritzen F. Fourier-accelerated nodal solvers (FANS) for homogenization problems. *Comput Mech*. 2018;62:359-392.
49. Ladecký M, Leute RJ, Falsafi A, et al. Optimal FFT-accelerated finite element solver for homogenization. *arXiv preprints*, arXiv:2203.02962. 2022.
50. Schneider M, Ospald F, Kabel M. Computational homogenization of elasticity on a staggered grid. *Int J Numer Methods Eng*. 2016;105(9):693-720.
51. Dorn C, Schneider M. Lippmann-Schwinger solvers for the explicit jump discretization for thermal computational homogenization problems. *Int J Numer Methods Eng*. 2019;118(11):631-653.
52. Pabst W, Uhlířová T, Gregorová E, Wiegmann A. Relative Young's modulus and thermal conductivity of isotropic porous ceramics with randomly oriented spheroidal pores—Model-based relations, cross-property predictions and numerical calculations. *J Eur Ceram Soc*. 2018;38(11):4026-4034.
53. Schneider M, Hofmann T, Andrä H, et al. Modeling the microstructure and computing effective elastic properties of sand core materials. *Int J Solids Struct*. 2018;143:1-17.
54. Uhlířová T, Pabst W. Conductivity and Young's modulus of porous metamaterials based on Gibson-Ashby cells. *Scr Mater*. 2019;159:1-4.
55. Schneider M. On the effective viscosity of a periodic suspension—Analysis of primal and dual formulations for Newtonian and Non-Newtonian solvents. *Math Methods Appl Sci*. 2016;39(12):3309-3327.
56. Bertóti R, Wicht D, Hrymak A, Schneider M, Böhlke T. A computational investigation of the effective viscosity of short-fiber reinforced thermoplastics by an FFT-based method. *European J Mech B Fluids*. 2021;90:99-113.
57. Schneider M. Lippmann-Schwinger solvers for the computational homogenization of materials with pores. *Int J Numer Methods Eng*. 2020;121(22):5017-5041.
58. Bonnet G. Effective properties of elastic periodic composite media with fibers. *J Mech Phys Solids*. 2007;55:881-899.
59. Vondřejc J. Improved guaranteed computable bounds on homogenized properties of periodic media by Fourier-Galerkin method with exact integration. *Int J Numer Methods Eng*. 2014;107:1106-1135.
60. Vondřejc J, Zeman J, Marek I. Guaranteed upper–lower bounds on homogenized properties by FFT-based Galerkin method. *Comput Methods Appl Mech Eng*. 2015;297:258-291.
61. Monchiet V. Combining FFT methods and standard variational principles to compute bounds and estimates for the properties of elastic composites. *Comput Methods Appl Mech Eng*. 2015;283:454-473.
62. Bhattacharya K, Suquet P. A model problem concerning recoverable strains of shape-memory polycrystals. *Proc Royal Soc A*. 2005;461:2797-2816.
63. Hashin Z, Shtrikman S. On some variational principles in anisotropic and nonhomogeneous elasticity. *J Mech Phys Solids*. 1962;10(4):335-342.
64. Hashin Z, Shtrikman S. A variational approach to the theory of the elastic behaviour of polycrystals. *J Mech Phys Solids*. 1962;10(4):343-352.
65. Hashin Z, Shtrikman S. A variational approach to the theory of the elastic behaviour of multiphase materials. *J Mech Phys Solids*. 1963;11(2):127-140.
66. Brisard S, Dormieux L. Combining Galerkin approximation techniques with the principle of Hashin and Shtrikman to derive a new FFT-based numerical method for the homogenization of composites. *Comput Methods Appl Mech Eng*. 2012;217–220:197-212.
67. Tu F, Jiao Y, Zhou X, Cheng Y, Tan F. The implementation of B-splines to Hashin and Shtrikman variational principle based FFT method for the homogenization of composite. *Int J Solids Struct*. 2020;191–192:133-145.
68. Gélébart L, Ouaki F. Filtering material properties to improve FFT-based methods for numerical homogenization. *J Comput Phys*. 2015;294:90-95.
69. Kabel M, Merkert D, Schneider M. Use of composite voxels in FFT-based homogenization. *Comput Methods Appl Mech Eng*. 2015;294:168-188.
70. Kabel M, Fink A, Schneider M. The composite voxel technique for inelastic problems. *Comput Methods Appl Mech Eng*. 2017;322:396-418.
71. Vondřejc J, Zeman J, Marek I. An FFT-based Galerkin method for homogenization of periodic media. *Comput Math Appl*. 2014;68:156-173.
72. Schneider M. Convergence of FFT-based homogenization for strongly heterogeneous media. *Math Methods Appl Sci*. 2015;38(13):2761-2778.
73. Ye C, Chung ET. Convergence of trigonometric and finite-difference discretization schemes for FFT-based computational micromechanics. *BIT Numer Math*. 2023;63:11.
74. Park C, Sheen D. P1-nonconforming quadrilateral finite element methods for second-order elliptic problems. *SIAM J Numer Anal*. 2003;41:624-640.
75. Ramière I. Convergence analysis of the Q1-finite element method for elliptic problems with non-boundary-fitted meshes. *Int J Numer Methods Eng*. 2008;75(9):1007-1052.
76. Schneider M, Wicht D. Superconvergence of the effective Cauchy stress in computational homogenization of inelastic materials. *Int J Numer Methods Eng*. 2023;124:959-978.

77. Schneider M. Superaccurate effective elastic moduli via postprocessing in computational homogenization. *Int J Numer Methods Eng*. 2023;123:4119-4135.
78. Ciarlet PG. *The Finite Element Method for Elliptic Problems*. North Holland; 1978.
79. Sendov B, Popov VA. *The Averaged Moduli of Smoothness*. Wiley; 1989.
80. DeVore RA, Lorentz GG. *Constructive Approximation*. Springer; 2003.
81. Saranen J, Vainikko G. *Periodic Integral and Pseudodifferential Equations with Numerical Approximation*. Springer; 2002.
82. Hristov VH. Best onesided approximations and mean approximations by interpolation polynomials of periodic functions. *Math Balk*. 1989;3:418-429.
83. Prestin J, Xu Y. Convergence rate of trigonometric interpolation for non-smooth functions. *J Approx Theory*. 1994;77:113-122.
84. Nikol'skii SM. *Approximation of Functions of Several Variables and Imbedding Theorems*. Springer; 1975.
85. Keshav S, Fritzen F, Kabel M. FFT-based homogenization at finite strains using composite boxels (ComBo). *Comput Mech*. 2022:1-22.
86. Zygmund A. *Trigonometric Series*. Vol I. Cambridge University Press; 1959.
87. Rudin W. *Real and Complex Analysis*. McGraw-Hill; 1966.
88. Weisz F. *Summability of Multi-Dimensional Trigonometric Fourier Series*. Springer; 2012.
89. Young WH. On the multiplication of successions of Fourier constants. *Proc Royal Soc A*. 1912;87(596):331-339.
90. Stein E. *Singular Integrals and Differentiability Properties of Functions*. Princeton University Press; 1970.
91. Li Y, Nirenberg L. Estimates for elliptic systems from composite material. *Commun Pure Appl Math*. 2003;56(7):892-925.
92. Ossendrijver M. Ancient Babylonian astronomers calculated Jupiter's position from the area under a time-velocity graph. *Science*. 2016;351(6272):482-484.
93. Trefethen LN, Weideman JAC. The exponentially convergent trapezoidal rule. *SIAM Rev*. 2014;56(3):385-458.
94. Atkinson KE. *An Introduction to Numerical Analysis*. 2nd ed. John Wiley & Sons; 1989.
95. Cruz-Uribe D, Neugebauer CJ. Sharp error bounds for the trapezoidal rule and Simpson's rule. *J Inequal Pure Appl Math*. 2002;3(4):49.
96. Verlinden P, Potts DM, Lyness JN. Error expansions for multidimensional trapezoidal rules with Sidi transformations. *Numer Algorithms*. 1997;16:321-347.
97. Neff P, Knees D. Regularity up to the boundary for nonlinear elliptic systems arising in time-incremental infinitesimal elasto-plasticity. *SIAM J Math Anal*. 2008;40(1):21-43.
98. Horgan CO. Korn's inequalities and their applications in continuum mechanics. *SIAM Rev*. 1995;37(4):491-511.
99. Evans LC. *Partial Differential Equations*. AMS; 1998.
100. Doghri I, Brassart L, Adam L, Gérard J-S. A second-moment incremental formulation for the mean-field homogenization of elasto-plastic composites. *Int J Plast*. 2011;27(3):352-371.
101. Kanatani K. Distribution of directional data and fabric tensors. *Int J Eng Sci*. 1984;22:149-164.
102. Advani SG, Tucker CL. The use of tensors to describe and predict fiber orientation in short fiber composites. *J Rheol*. 1987;31:751-784.
103. Schneider M. The sequential addition and migration method to generate representative volume elements for the homogenization of short fiber reinforced plastics. *Comput Mech*. 2017;59:247-263.
104. Montgomery-Smith S, He W, Jack D, Smith D. Exact tensor closures for the three-dimensional Jeffery's equation. *J Fluid Mech*. 2011;680:321-335.
105. Hashin Z. The elastic moduli of heterogeneous materials. *J Appl Mech*. 1962;29(1):143-150.
106. Wicht D, Schneider M, Böhlke T. An efficient solution scheme for small-strain crystal-elasto-viscoplasticity in a dual framework. *Comput Methods Appl Mech Eng*. 2020;358:112611.
107. Bellis C, Moulinec H, Suquet P. Eigendecomposition-based convergence analysis of the Neumann series for laminated composites and discretization error estimation. *Int J Numer Methods Eng*. 2020;121:201-232.
108. Brisard S, Legoll F. Periodic homogenization using the Lippmann–Schwinger formalism. *arXiv preprint*, arXiv:1411.0330v1. 2014.
109. Dauge M. *Elliptic Boundary Value Problems on Corner Domains: Smoothness and Asymptotics of Solutions*. Springer; 2003.
110. Mazzucato AL, Nistor V. Well-posedness and regularity for the elasticity equation with mixed boundary conditions on polyhedral domains and domains with cracks. *Arch Ration Mech Anal*. 2010;195(1):25-73.

How to cite this article: Schneider M. On the effectiveness of the Moulinec–Suquet discretization for composite materials. *Int J Numer Methods Eng*. 2023;124(14):3191-3218. doi: 10.1002/nme.7244

APPENDIX A. DERIVATION OF THE REPRESENTATION OF THE QUADRATURE ERROR IN ONE SPATIAL DIMENSION

The purpose of this appendix is to show the validity of equation (48), that is, for any natural number $N \in \mathbb{N}$ there is a function $w_N : [0, 2\pi] \to \mathbb{R}$, bounded uniformly in N, s.t., for any continuous and periodic function $f : [0, 2\pi] \to \mathbb{R}$ with

integrable weak derivative f' the representation

$$\frac{1}{N}\sum_{j=1}^{N} \fint \left(\frac{2\pi\, j}{N}\right) = \fint_0^{2\pi} f(x)\, dx + \frac{1}{N}\fint_0^{2\pi} f'(x)\, w_N(x)\, dx \tag{A1}$$

holds, where $\fint$ refers to the mean integral.

For $0 \le a < b \le 2\pi$ one observes, by the fundamental theorem of calculus,

$$\int_a^b \frac{d}{dx}\left(f(x)\frac{1}{2}\frac{2x-a-b}{b-a}\right)\, dx = \frac{1}{2}\left(f(a)+f(b)\right). \tag{A2}$$

On the other hand, the product rule gives

$$\int_a^b \frac{d}{dx}\left(f(x)\frac{1}{2}\frac{2x-a-b}{b-a}\right)\, dx = \int_a^b f'(x)\frac{1}{2}\frac{2x-a-b}{b-a}\, dx + \frac{1}{b-a}\int_a^b f(x)\, dx, \tag{A3}$$

that is, the compact formula

$$\frac{b-a}{2}\left(f(a)+f(b)\right) = \int_a^b f(x)\, dx + \int_a^b f'(x)\frac{2x-a-b}{2}\, dx. \tag{A4}$$

For $a = 2\pi j/N$ and $b = 2\pi(j+1)/N$ $(j = 0, \dots, N-1)$, this formula becomes

$$\frac{2\pi}{2N}\left(f\left(\frac{2\pi j}{N}\right)+f\left(\frac{2\pi(j+1)}{N}\right)\right) = \int_{2\pi j/N}^{2\pi(j+1)/N} f(x)\, dx + \int_{2\pi j/N}^{2\pi(j+1)/N} f'(x)\frac{Nx-\pi(2j+1)}{N}\, dx. \tag{A5}$$

Summing up from $j = 0$ to $j = N-1$ gives equation (48) with the piece-wise defined function

$$w_N(x) = Nx - \pi(2j+1), \quad 2\pi j/N \le x \le 2\pi(j+1)/N. \tag{A6}$$

The function w_N is piecewise linear and satisfies the N-independent bound

$$|w_N(x)| \le \pi, \quad x \in [0, 2\pi]. \tag{A7}$$

APPENDIX B. DERIVATION OF THE HIGHER GRADIENT BOUNDS IN THE INTERPOLATION ESTIMATE

The goal of this appendix is to show the estimate (86)

$$\left\|\nabla^k\left(\phi_N\mathbb{C} : F_N\boldsymbol{\varepsilon}\right)\right\|_{L^2(\mathrm{Y}^d)} \lesssim N^{k-\frac{1}{2}} \tag{B1}$$

required in Section 3.3. The product rule implies

$$\left\|\nabla^k\left(\phi_N\mathbb{C} : F_N\boldsymbol{\varepsilon}\right)\right\|_{L^2(\mathrm{Y}^d)} \lesssim \left\|\phi_N\nabla^k(F_N\boldsymbol{\varepsilon})\right\|_{L^2(\mathrm{Y}^d)} + \sum_{\ell=1}^{k}\left\|\nabla^\ell\left(\phi_N\mathbb{C}\right)\right\|_{L^2(\mathrm{Y}^d)}\left\|\nabla^{k-\ell}\left(F_N\boldsymbol{\varepsilon}\right)\right\|_{L^\infty(\mathrm{Y}^d)}. \tag{B2}$$

For the first term, we observe

$$\left\|\phi_N\nabla^k(F_N\boldsymbol{\varepsilon})\right\|_{L^2(\mathrm{Y}^d)} \le \left\|\nabla^k(F_N\boldsymbol{\varepsilon})\right\|_{L^2(\mathrm{Y}^d)} \lesssim N^{k-1}\ \left\|\nabla(F_N\boldsymbol{\varepsilon})\right\|_{L^2(\mathrm{Y}^d)} \tag{B3}$$

by the L^2-Bernstein estimate (35). We split the term

$$\left\|\nabla(F_N\boldsymbol{\varepsilon})\right\|_{L^2(\mathrm{Y}^d)} \le \left\|\nabla F_N[(1-\phi_N)\boldsymbol{\varepsilon}]\right\|_{L^2(\mathrm{Y}^d)} + \left\|\nabla F_N[\phi_N\boldsymbol{\varepsilon}]\right\|_{L^2(\mathrm{Y}^d)}. \tag{B4}$$

For the first contribution, we utilize the Bernstein estimate (35), the boundedness of the Féjer means and the convergence-rate estimate (46)

$$\begin{aligned}\|\nabla F_N[(1-\phi_N)\boldsymbol{\varepsilon}]\|_{L^2(\mathrm{Y}^d)} &\lesssim N\,\|F_N[(1-\phi_N)\boldsymbol{\varepsilon}]\|_{L^2(\mathrm{Y}^d)}\\ &\leq N\,\|(1-\phi_N)\boldsymbol{\varepsilon}\|_{L^2(\mathrm{Y}^d)}\\ &\leq N\,\|(1-\phi_N)\|_{L^2(\mathrm{Y}^d)}\,\|\boldsymbol{\varepsilon}\|_{L^\infty(\mathrm{Y}^d)}\\ &\lesssim N^{\frac{1}{2}}.\end{aligned} \tag{B5}$$

To treat the second term, we notice that taking the gradient commutes with Féjer approximation,

$$\|\nabla F_N[\phi_N\boldsymbol{\varepsilon}]\|_{L^2(\mathrm{Y}^d)} = \|F_N\,[\nabla(\phi_N\boldsymbol{\varepsilon})]\|_{L^2(\mathrm{Y}^d)} \leq \|\nabla(\phi_N\boldsymbol{\varepsilon})\|_{L^2(\mathrm{Y}^d)} \lesssim N^{\frac{1}{2}}, \tag{B6}$$

where the last estimate is obtained as a part of argument (81). Thus, we are let to the bound

$$\|\nabla(F_N\boldsymbol{\varepsilon})\|_{L^2(\mathrm{Y}^d)} \lesssim N^{\frac{1}{2}}, \tag{B7}$$

which, in turn, leads to the expression

$$\left\|\phi_N\nabla^k(F_N\boldsymbol{\varepsilon})\right\|_{L^2(\mathrm{Y}^d)} \lesssim N^{k-\frac{1}{2}}. \tag{B8}$$

For the second term in the estimate (B2), we observe

$$\left\|\nabla^\ell\,(\phi_N\mathbb{C})\right\|_{L^2(\mathrm{Y}^d)} \lesssim N^{\ell-\frac{1}{2}} \tag{B9}$$

as a consequence of estimate (45) for $k = |\alpha|$ as well as $p = 2$, and

$$\left\|\nabla^{k-\ell}\,(F_N\boldsymbol{\varepsilon})\right\|_{L^\infty(\mathrm{Y}^d)} \lesssim N^{k-\ell}\,\|F_N\boldsymbol{\varepsilon}\|_{L^\infty(\mathrm{Y}^d)} \leq N^{k-\ell}\,\|\boldsymbol{\varepsilon}\|_{L^\infty(\mathrm{Y}^d)} \tag{B10}$$

using the Bernstein estimate (32) and the conservation of boundedness offered by the Féjer means (25). The latter two estimates combine to the bound

$$\left\|\nabla^\ell\,(\phi_N\mathbb{C})\right\|_{L^2(\mathrm{Y}^d)}\left\|\nabla^{k-\ell}\,(F_N\boldsymbol{\varepsilon})\right\|_{L^\infty(\mathrm{Y}^d)} \lesssim N^{k-\frac{1}{2}}. \tag{B11}$$

Thus, in view of the contributions (B8) and (B11), the estimate (B2) implies the statement (B1), which was to be shown.

DOI: 10.1002/nme.7244
URN: urn:nbn:de:hbz:465-20240711-105613-6